Compressive Radar Cross Section Computation

by

Xiang Li

A thesis submitted to the Ottawa Carleton Institute for Electrical and Computer Engineering
in partial fulfillment to the thesis requirement for the degree of

Master of Applied Science

in

Electrical and Computer Engineering

uOttawa

University of Ottawa
Ottawa, Ontario, Canada

Abstract

Compressive Sensing (CS) is a novel signal-processing paradigm that allows sampling of sparse or compressible signals at lower than Nyquist rate. The past decade has seen substantial research on imaging applications using compressive sensing. In this thesis, CS is combined with the commercial electromagnetic (EM) simulation software newFASANT to improve its efficiency in solving EM scattering problems such as Radar Cross Section (RCS) of complex targets at GHz frequencies. This thesis proposes a CS-RCS approach that allows efficient and accurate recovery of under-sampled RCSs measured from a random set of incident angles using an accelerated iterative soft thresh-holding reconstruction algorithm. The RCS results of a generic missile and a Canadian KingAir aircraft model simulated using Physical Optics (PO) as the EM solver at various frequencies and angular resolutions demonstrate good efficiency and accuracy of the proposed method.

Acknowledgements

The realization of this thesis would not have been possible without the support of many – my sincere thanks to all of them for being part of the journey. My inspiration of studying Electromagnetics first started when I was working for the Defence Research and Development Canada – Ottawa Research Centre, where I was fortunate enough to meet my thesis co-supervisor Dr. Chen Wu who manifests great positivity and passion in his works. I owe my gratitude to my professor Dr. Mustapha C.E. Yagoub, who is detail-oriented and always encourages students around him to strive for the highest. Same as many other life events – a series of seemingly non-related coincidences intervene in the future and become deciding factor of one's value and career – the Master's program at the University of Ottawa helped define who I am today. I was honoured to study under Dr. Yagoub and Dr. Wu. I sincerely thank my thesis supervisors for their selflessness and guidance and DRDC for their financial supports.

Finally, I extend my deep and sincere gratitude to my family and friends for their unconditional support and unparalleled love. I am forever grateful to my parents, without whom this journey would not have been possible.

Contents

List of Figures

List of Tables

List of Acronyms

Acronym	Definition
BP	Basis Pursuit
BPDN	Basis Pursuit De-Noising
CEM	Computational Electromagnetics
CS	Compressive (or Compressed) Sensing
CoSaMP	Compressive Sensing Orthogonal Matching Pursuit
DCT	Discrete Cosine Transform
DFT	Discrete Fourier Transform
EM	Electromagnetic
FFT	Fast Fourier Transform
HP	Hermite Polynomial
MLFMA	Multilevel Fast Multipole
MoM	Method of Moments
OMP	Orthogonal Matching Pursuit
PO	Physical Optics
RCS	Radar Cross Section
ROMP	Regularized Orthogonal Matching Pursuit
RIP	Restricted Isometry Property
SpaRSA	Sparse Reconstruction by Separable Approximation

List of Symbols

Symbol	Definition
$\boldsymbol{A}$	Measurement Matrix
$\boldsymbol{E}$	Radar Cross Section Signal
$\boldsymbol{E_s}$	Far-zone Scattered Electric Field
$\boldsymbol{I}$	Basis Expansion Coefficients
$\boldsymbol{I_{CS}}$	Under-sampled Basis Expansion Coefficients
$\boldsymbol{J}$	Currents
K	Sparse Signal Length
N	Original Signal Length
$\boldsymbol{P}$	Basis Expansion Function
$\boldsymbol{r}$	Residual
$\mathbf{s}$	Sparse Representation of the Original Signal
$\boldsymbol{\theta_{CS}}$	Compressed Incident Angle
t	Step Size
τ	Regularization Parameter
$\boldsymbol{\Phi}$	Sensing Matrix
$\boldsymbol{x}$	Orignal Signal
λ	Noise Level
$\boldsymbol{\Psi}$	Transformation Matrix
$\boldsymbol{\theta}$	Original Incident Angle

Chapter 1 Introduction

1.1 Motivations

Human brains choose to memorize what is important, instead of overloading themselves with overwhelmingly detailed information. While it is very unlikely to imprint every fine detail of an object into our brains, an object's general signatures such as orientation, colour and smell can be quickly registered and stored away in our memory folders. Every memory unit, whether in digital or physical form, naturally requires information compression due to limited storing resources. In the digital world, a common practice for compressing a signal is to reduce redundancy and triviality. Conventionally, to compress any digital signal, including audio, video and radar signals, one first needs to capture every frame of the signal in accordance with the well-established Nyquist-Shannon sampling theory in order to identify and locate what is important in the information received and discard the unnecessary parts. However, this sample-then-compress process can be inefficient as the full-length of the signal must be stored first. Now, imagine a compress-then-sample process where we only need to acquire and store the most important information that is often only a fraction of the original signal. The compress-then-sample process not only saves already limited storing resources but also allows the compressed signals to travel faster (e.g., file transfer over the internet). Similar to the conventional signal compression, the original signal can be recovered and reconstructed.

This fascinating idea did not become famous overnight. Quite the opposite, it had been long treated as an impossible and ill-posed problem for quite some time. Simply put, there is no unique solution. The idea was left unattended until the mathematical foundations of Compressed (or Compressive) Sensing (CS) were established by [1][2][3][4][5][6]. Compressive Sensing, as its name suggests, allows one to compress signals from the very beginning of signal acquisition stage where only important information is acquired and stored. Finally, the compressed signals are recovered using an appropriate reconstruction algorithm. Along with the fast-growing industry for Computer Vision, researchers (including Donoho [2], Tao [3], etc.) have mainly exploited Compressive Sensing in imaging applications.

This thesis exploits Compressive Sensing in Computational Electromagnetics, especially in computing high-resolution Radar Cross Sections. Also, it studies different factors such as electromagnetic solver (i.e. numerical or asymptotic), structure complexity, transformation bases, and reconstruction algorithms that influence the reconstruction accuracy using some CS-based methods.

Since the discovery of Compressive Sensing (CS), it has quickly become one of the bandwagons of data acquisition and compression paradigm. CS allows near-optimal reconstruction from an incomplete data set that is either sparse in its original domain or a transformation domain. Unlike the well-established Nyquist sampling theorem, CS utilizes a non-linear sampling process that allows a faster sampling rate with fewer measurements than the traditional linear sampling process [2]. CS has also been used as an effective de-noising method in digital image and audio processing. Throughout the past decade, applications such as single-pixel camera by Rice University [1], medical imaging [7] (i.e. magnetic resonance imaging (MRI)), and seismic imaging [8] have been developed or improved using CS-based techniques [5]. Although the use of CS has been mainly focused on imaging applications, recent CS studies on radar localization and computational electromagnetics (CEM) have shown promising results [9], [10]. However, one of the major concerns for CEM applications is that it is computationally costly to calculate the RCS of electronically large objects [11].

Numerical methods such as the full-wave analysis method – Method of Moments[12] and its variation such as multilevel fast multipole (MLFMA) [13] are capable of accurate RCS calculation but suffer from computational time. Therefore, asymptotic methods such as physical optics (PO) [14] are regarded as good alternatives for high-frequency RCS calculation, especially for large targets. In this context, researchers in the field of computational electromagnetics have been focusing on solving RCS problems by both numerical and analytical means ever since the 90s. Recent breakthrough on compressive sensing has shined the light on efficiently solving the RCS problems using signal-processing approaches [9][15][16]. The use of compressive sensing, combined with numerical or analytical EM solver, has the potentials to improve the efficiency in solving RCS problems [15]. Signal reconstruction quality varies because of: 1) the measurements – a randomly selected fraction of signal will imply covering the most prominent coefficients of the

original signal differently each time, and 2) the nature of the reconstruction algorithms, especially the greedy and l_1 methods that are popularly used in CS[17]. In EM modelling, direction with high RCS magnitude often pose greater concerns than the nulls.

1.2 Contributions

This thesis highlights the use of CS in radar cross-section computations, which play a significant role in electromagnetic modelling and other radar electronic warfare applications. This work improves the efficiency of RCS computation of complex targets such as a real-life aircraft model at GHz frequencies using a CS-based framework combined with a commercial EM software – newFASANT. The research investigates the RCS computation speed and reconstruction quality by comparing different types of CS usages, transformation bases and reconstruction algorithms.

Therefore, the following contributions can be highlighted for this work:

- To the best of the authors' knowledge, this work associates, for the first time, RCS resolution, frequency and geometry complexity as deciding factors with the compressibility of scattering signals. Previously, most studies used Greedy methods for signal reconstruction and assumed *a priori* information such as signal sparsity and smooth functions. This thesis proposes an accelerated iterative thresholding algorithm, Sparse Reconstruction by Separable Approximation (SpaRSA), which does not require signal sparsity and works with non-smooth signals. In addition, various transformation bases, as well as reconstruction algorithms, are under scrutiny for a most accurate solution.

- As opposed to the conventional CS approaches in CEM applications that extract currents and far-zone electric fields just by computing RCS, a new approach CS-RCS – was proposed to directly utilize the more compressible RCS signal as the signal of interest. The CS-RCS approach can be conveniently combined with various EM field solvers to calculate under-sampled RCS from pre-determined directions and provides superior efficiency and reconstruction accuracy compared to the conventional CS approaches.

- A MATLAB script that automatically calculates the convergence of the recovered RCS signals by accumulating non-repetitive measurements was developed. Naturally, the sparsity of signals and the number of measurements required for reconstruction are unknown to operators. The script mandates to find the ideal quality of signal reconstruction using a minimum number of measurements.

1.3 Thesis Organization

Chapter 1 discusses a general theoretical framework for CS with possible CS usages in electromagnetics and essential mathematical concepts for CS establishment.

While most image signals provide concise representation, Chapter 2 discusses the implementation and potential of MATLAB-based CS algorithm for improving the efficiency of electromagnetic scattering problems. The sparsity of signals, choice of measurement matrices and transformation bases establish the fundamentals and feasibility of CS in a given application.

In Chapter 3, a literature review of CS for CEM applications and inverse scattering problems is conducted, concluding that two conventional CS approaches can be used namely, the current approach (where CS is applied to the currents in the MoM matrix equation) and the scattering-field approach (where CS is applied to the far-zone scattered fields using asymptotic methods for electronically-large objects). This chapter also proposes a novel CS-RCS approach where, instead of the scattered fields, the RCS data is the signal of interest.

Chapter 4 provides detailed simulation procedures and numerical results while comparing between different transformation bases, reconstruction algorithms at various frequencies for several objects with different structural-complexity. The results show that the CS-RCS approach, when incorporated with the SpaRSA algorithm is capable of improving the efficiency of RCS computation with good accuracy.

Chapter 5 draws a conclusion and provides directions for future work of the proposed CS-RCS solution for efficient RCS computation.

1.4 Publications

- X. Li and M.C.E Yagoub, "RCS of complex targets via compressive sensing," *IEEE International Symposium on Antennas and Propagation and USNC-URSI Radio Science Meeting,* Atlanta, GA, pp. 1-2, July 2019.
- X. Li, M.C.E. Yagoub, "Cavity-backed spiral antenna design and mutual coupling study in closely spaced arrays," *Defence Research and Development Canada*, Internal Report, Part III, March. 2019. 24 pages.
- X. Li and M.C.E Yagoub, "Computation electromagnetic modelling for spiral antenna array and aircraft radar cross section," *Defence Research and Development Canada,* Internal Report, Feb. 2019
- X. Li, M.C.E. Yagoub, "Cavity-backed spiral antenna design and mutual coupling study in closely spaced arrays," *Defence Research and Development Canada*, Internal Report, Part II, Oct. 2018. 54 pages.
- X. Li and M.C.E Yagoub, "Compressive sensing for computational electromagnetics," *Ottawa-Artificial Intelligence Workshop*, National Research Council, ON, October 2019.
- X. Li and M.C.E Yagoub, "Wideband cavity-backed spiral antenna design and mutual coupling study in a closely-spaced array," *IEEE 18th Symposium on Antenna Technology and Applied Electromagnetics*, Waterloo, ON, pp. 1-4, Aug. 2018.
- X. Li, M.C.E. Yagoub, "Cavity-backed spiral antenna design and mutual coupling study in closely spaced arrays," *Defence Research and Development Canada*, Internal Report, Part I, March 2018. 33 pages.
- X. Li and M.C.E Yagoub, "Ultra-wideband cavity-backed spiral antenna design and mutual coupling study between multiple elements," *10th Annual Electrical and Computer Engineering Graduate Poster Competition,* University of Ottawa, ON, March 2018.
- X. Li and M.C.E Yagoub, "Spiral antenna array study and King Air aircraft radar cross section calculation: A report on radar electronic warfare modelling and simulation and hardware-in-the-loop," *Defence Research and Development Canada,* Internal Publication, Contract Report.

Chapter 2 Compressive Sensing Theory

Conventionally, data are sampled uniformly at the Nyquist rate in accordance with the Shannon-Nyquist sampling theorem. As a result, redundant information is acquired and stored during the acquisition stage and discarded during compression. In addition, the Nyquist sampling rate may not be practical for real-life applications such as analog-to-digital converter when the sampling rate exceeds the hardware specification by orders of magnitudes[18]. Over a decade ago, Donoho, Candes, and Tso published a series of papers, which built the mathematical foundation of compressive sensing [2][3][4][19][20][21]. They proposed that CS provides a near-optimal success rate of perfect reconstruction for signals that have concise representation in a transformation domain. Since most natural signals and some synthetic signals can be found sparse in a transformation domain, CS has been studied across a wide range of interests. Note that this thesis discusses discrete-time CS exclusively as there is a lack of mathematical foundations for the continuous-time CS [6]. The advantage of the CS framework is twofold: 1) efficient acquisition of large volume of data (CS enables non-linear sampling with minimal measurements for signals that are sparse or sparse in a transformation domain) and, 2) Efficient data processing (only a fraction of original data is processed since very few data are needed) [2]. Since only a small set of measurements are acquired, the entire signal needs to be reconstructed. However, traditional methods such as interpolation cannot be applied to non-stationary signals [22] and only fit certain signal models. Hence, CS utilizes optimization instead of interpolation for signal recovery.

2.1 Sparsity

Sparse representations are found in many natural and synthetic signals when expressed in a transformation domain. Consider a one-dimensional (1D) finite length and discrete-time column vector $\boldsymbol{x} = [x_1, x_2 \cdots, x_N]^T$, $\boldsymbol{x} \in R^N$. Here the superscript "T" denotes transposition. The signal $\boldsymbol{x}$ can be expanded in a basis such as an orthonormal basis $\boldsymbol{\Psi} = [\psi_1, \psi_2 \cdots, \psi_N]^T$. Later sections will briefly explain different transformation bases and why the orthonormal basis is generally preferred [23].

The signal $\boldsymbol{x}$ can be expressed with respect to $\boldsymbol{\Psi}$ as:

$$\boldsymbol{x} = \sum_{i=1}^{N} s_i \psi_i \ \ or \ \boldsymbol{x} = \boldsymbol{\Psi s} \tag{2-1}$$

where $\boldsymbol{s} = [s_1, s_2 \cdots, s_N]^T$ is the vector that contains weighting coefficients of ${\psi_i}^T \boldsymbol{x}$. We call such a signal $\boldsymbol{x}$ as K sparse when it is a linear combination of only K basis coefficients. The column vector $\boldsymbol{s}$ only contains K non-zero coefficients with the rest of the N-K coefficients set to zero [6]. Note that not all sparse signals can be easily identified as sparse in their original domain. One often needs to transform such signals into their sparse domain to examine their sparsity. For instance, let us assume a signal $\boldsymbol{x}$ with length N=361. The signal is the summation of two sinusoids $\boldsymbol{x}1 = \sin(2\pi f_1)$ and $\boldsymbol{x}2 = \sin(2\pi f_2)$, where $f_1 = 6$ and $f_2 = 18$. Each real-valued sinusoid should have two non-zero components in the frequency domain. As shown in Figure 1, the signal $\boldsymbol{x}$ indeed has 4 peaks. Therefore the signal is called K=4 sparse in the Fourier frequency domain; thus, perfect reconstruction is possible.

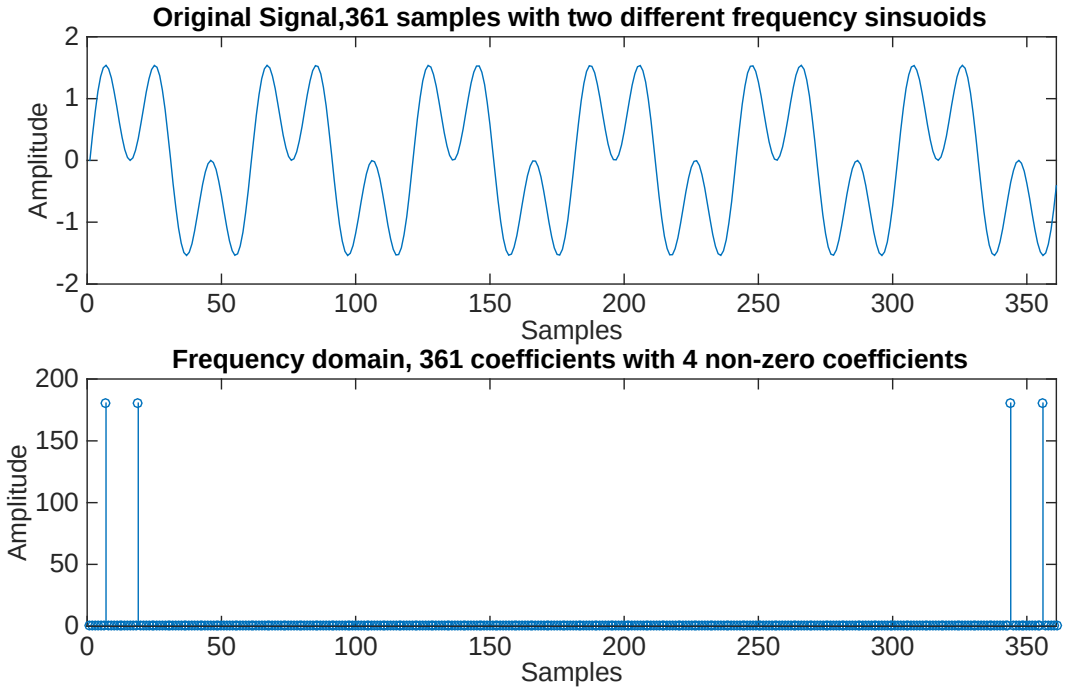

Figure 1 - Signal representation in the sparse domain

In reality, signals in many applications such as scattering problems are not strictly sparse but rather 'compressible' – that is when the signal consists of a few large coefficients and many small coefficients. The decay rate determines the compressibility of *E*. Compressibility is the measure of how compressible a signal is and will be discussed in the following section. Depending on the compressibility of a compressible signal, it can often be recovered accurately when a proper reconstruction method is used [24].

2.2 The Conventional Transform Coding Problem

In fact, the idea of approximating compressible and sparse signals is not new. The foundation of transform coding, which has long been integrated into day-to-day data acquisition applications such as digital cameras, is used substantially in the digital world. The procedure for transform coding is as follows:

1. Acquire full-length original signal $\boldsymbol{x}$
2. Calculate the transform coefficients $\boldsymbol{s}$ by taking the product between the transpose of a transformation basis $\boldsymbol{\Psi}$ and signal $\boldsymbol{x}$
3. Locate the K largest coefficients and discard the N-K small coefficients
4. Encode the values and the locations of K largest coefficients
5. Reconstruct the transform coefficients using the pseudo-inversion:

$$\boldsymbol{s} = (\boldsymbol{A}^T\boldsymbol{A})^{-1}\boldsymbol{A}^T\boldsymbol{y} \tag{2-3}$$

This process is redundant and inefficient because the entire set of the original signal must not only be acquired but also temporarily stored [6]. Then, the signal's coefficients are sorted from the largest to the smallest. Compression takes place when the K largest coefficients are kept while the rest N-K coefficients are thrown away.

Figure 2 - Conventional transform coding scheme

This type of coding scheme is well established and plays an important role in digital image compression, such as the JPEG standard. JPEG is a lossy compression instead of a lossless compression method. High-quality image with little perceptible loss can be achieved if proper transformation basis and low degree of compression are selected.

2.3 Compressive Sensing Paradigm

Since only a few samples of a signal are useful, and the majority are discarded, compressive sensing allows one to bypass the inefficient process of acquiring full-length signals by under-sampling the signals in a deliberate way.

Consider to only acquiring M (M ≪ N) measurements of the signal $\boldsymbol{x}$ according to an MxN sensing matrix $\boldsymbol{\Phi}$:

$$\boldsymbol{y} = \boldsymbol{\Phi x} = \boldsymbol{\Phi \Psi s} = \boldsymbol{As} \tag{2-2}$$

where $\boldsymbol{A}$ is an MxN measurement matrix, and $\boldsymbol{y}$ is the vector of available samples measured from the signal $\boldsymbol{x}$. This $\boldsymbol{y} = \boldsymbol{As}$ is an ill-posed problem in general that sometimes makes users first skeptical but later surprised about the whole idea of CS. Such a system may have an infinite number of solutions, as there may be an infinite number of $\boldsymbol{s}$ for $\boldsymbol{y} = \boldsymbol{As}$. However, CS aims to find the sparsest solution. Following illustrates the process of CS in general:

1. Select the appropriate measurement matrix $\boldsymbol{\Phi}$ and transformation matrix $\boldsymbol{\Psi}$
2. Acquire measured signal *y* that contains available samples of original signal x according to $\boldsymbol{\Phi}$
3. Reconstruct the transform coefficient $\boldsymbol{s}$ using non-linear iterative optimization
4. Obtain the approximated original signal $\boldsymbol{x}$ by substituting $\boldsymbol{s}$ to equation (2-1)

In contrast to the traditional transform coding problem, CS is more efficient by acquiring only the significant samples of the signal without prior knowledge of their locations. However, the location of the non-zero or zero coefficients is unknown *a priori*. Thus, the measurement is not adaptive and non-linear, and the sensing matrix $\boldsymbol{\Phi}$ is fixed and independent of the transformation matrix $\boldsymbol{\Psi}$ and the original signal $\boldsymbol{x}$.

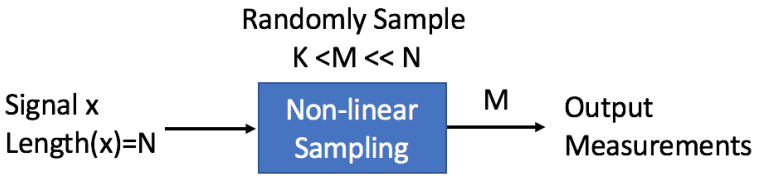

Figure 3 - Traditional compression process

Both the traditional and compressive sensing approaches require the compressed signal to be reconstructed (or recovered). Reconstruction for the traditional scheme, such as JPEG, is a simple linear operation that does not require *a priori* information. Generally, the goal of reconstruction/recovery in CS is to identify the largest coefficients and their corresponded locations in a signal from a limited number of random measurements. For this, *a priori* information is often demanded by many reconstruction algorithms. When applied to a frequency-sparse signal, reconstruction algorithms determine at approximately what frequency range, the largest transform coefficients can be observed [22].

2.4 Choice of Measurement Matrix

This section discusses the important factors that need to be taken into consideration when choosing an appropriate pair of $\boldsymbol{\Phi}$ and $\boldsymbol{\Psi}$ for any CS system.

2.4.1 Restricted Isometry Property

Choosing a stable pair of $\boldsymbol{\Phi}$ and $\boldsymbol{\Psi}$ or a measurement matrix $\boldsymbol{A}$ is significant for reconstruction quality and probability in CS. CS achieves data compression by dimensional reduction: information transfer from a high dimensional space to a low dimensional space. Any two independent arbitrary vectors from a high dimensional space can be confused and mapped to the same point in a low dimensional space. This causes information loss without information

preservation guarantees. This brings up a very important notion, the Restricted Isometry Property (RIP) that defines the robustness of CS given a pair of $\boldsymbol{\Phi}$ and $\boldsymbol{\Psi}$. RIP ensures information preservation, if the two vectors are sparse with close to orthogonal column with their Euclidean distance preserved. Studies have concluded RIP property as given a measurement matrix $\boldsymbol{A}$ and the isometry constant $\varepsilon > 0$, follow the wing equation holds for all K-sparse vectors $\boldsymbol{s}$ [3].

$$1 - \varepsilon \leq \frac{\|As\|_{l_2}^2}{\|s\|_{l_2}^2} \leq 1 + \varepsilon \tag{2-4}$$

while ε is not too close to 1, this property approximately guarantees that no any two K-sparse vectors $\boldsymbol{x}$ can relate to the same measurement vector $\boldsymbol{y}$, and thus every set of measurement results in a unique K-sparse vector [6]. Furthermore, [23] proposed that:

1. $if\ \varepsilon < 1, the\ K\ sparse\ vector\ \boldsymbol{x}\ has\ a\ unique\ solution\ by\ solving\ a\ l_0\ problem$
2. $if\ \varepsilon < \sqrt{2} - 1, the\ convex\ relaxation\ is\ exact$

However, it is hard to determine the isometry constant and to prove the RIP of a given pair of sensing and transformation matrices. Researchers have relied on the incoherence property to calculate if unique solution can be achieved using the pair.

2.4.2 Incoherence

The incoherence property of a measurement matrix is equally important as the RIP when selecting a measurement matrix that guarantees a high probability of reconstruction of sparse signals. Specifically, the incoherence of measurement matrix A refers to the incoherence of the sensing matrix $\boldsymbol{\Phi}$ and the transformation basis $\boldsymbol{\Psi}$:

$$\mu(\boldsymbol{A}) = max_{i \neq j, 1 \leq i,j \leq N} \left|\langle \boldsymbol{A}_i, \boldsymbol{A}_j \rangle\right| \ or\ \mu(\boldsymbol{\Phi}, \boldsymbol{\Psi}) = \sqrt{n} \cdot max_{i \neq j, 1 \leq i,j \leq N} \left|\langle \boldsymbol{\Phi}_i, \boldsymbol{\Psi}_j \rangle\right| \tag{2-5}$$

where *i* and *j* represent the column and row vectors, respectively. In order for the measurement matrix to be incoherent ($\mu(\boldsymbol{\Phi}, \boldsymbol{\Psi})$=1) any two elements of the matrix must be uncorrelated. The relationship between coherence and the number of samples required for signal recovery can be

represented as $M \geq cKlog(N)\mu^2(\boldsymbol{\Phi}, \boldsymbol{\Psi})$, where c is a constant [24]. This implies that a less coherent measurement matrix contributes to fewer measurements (or samples) for signal recovery[25]. Therefore, if the measurement matrix satisfies RIP and incoherence properties, where $\mu^2(\boldsymbol{\Phi}, \boldsymbol{\psi})$ is infinitely close to or equal to 1, a K-sparse signal of length N is recoverable from only $M \geq cKlog(\frac{N}{K}) \ll N$ [6].

Randomness plays an essential role in finding a good sensing matrix $\boldsymbol{\Phi}$. There are numerous possibilities of such random matrices such as independent and identically distributed (i.i.d) symmetric Bernoulli distribution, Gaussian measurement matrix (zero mean and 1/N variance Gaussian probability distribution) and other sub-Gaussian distributions [25]. These random sensing matrices also preserve high incoherence with most popular basis transformation matrices such as fast Fourier transform (FFT), Discrete Cosine Transform (DCT), Hermite Polynomial (HP) transform and wavelet transform matrices. In this thesis, we introduce the uniform sampling matrix that not only satisfies the RIP property with a large variety of transformation bases but also avoids redundancy in CEM applications [15]:

$$\begin{bmatrix} 0 & 1 & \dots & 0 \\ 1 & 0 & \cdots & 0 \\ \vdots & \vdots & \vdots & \vdots \\ 0 & 0 & \dots & 1 \end{bmatrix}$$

In a uniform sampling matrix, there exists only one non-zero element in each row while the location of the non-zero element is random. As a result, each row only provides one direction when multiplied with a direction vector.

2.5 Compressibility

As the work has a strong focus on CS for real-life applications, it is important to bring up the definition of signal compressibility because many real-life signals are not sparse in a strict sense in some given transformation bases. However, compressible signals can be reconstructed to a satisfactory level with very high possibility. A compressible signal comprises of coefficients decay rapidly like a power-law when sorted in descending order [3]. The compressibility of a

compressible signal $\boldsymbol{x_c}$ is governed by p ($p > 0$) and a constant R for n between 1 to N as indicated in the following equation:

$$|x_n| \leq R \cdot n^{-\frac{1}{p}} \tag{2-6}$$

Graphically, it is convenient to observe signal compressibility by observing the sorted coefficients of a signal. Figure 4 depicts the compressibility of a signal in certain sparse domain graphically.

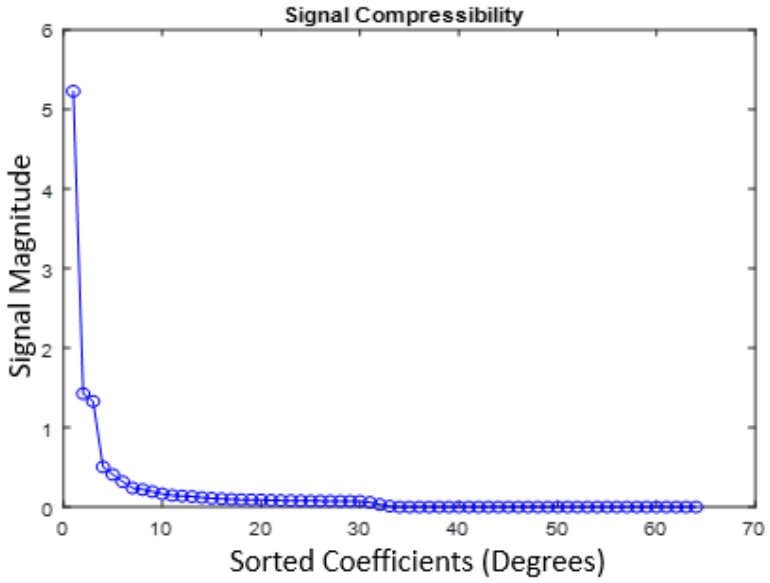

Figure 4 - Signal compressibility demonstration

Most natural and synthetic signals are not sparse in their original domains. In fact, a transformation domain determines whether a signal can be accurately reconstructed, although it may seem to be natural to blame the signals themselves for lack of concise representations. When represented in different transformation domains, the compressibility of a signal varies drastically. Therefore, to increase a signal's compressibility, one needs to start with a suitable transformation basis. In this thesis, especially in Chapter 4, the graphical representation of a given signal's compressibility in certain transformation basis is used extensively and has been proven as an effective way of predicting the reconstruction quality.

2.6 Transformation Basis

Finding an appropriate transformation basis where a signal appears to be sparse is the first and challenging step to apply CS to solve an RCS computation problem. There are some well-established transformation bases known for certain applications. In fact, transformation basis plays a significant role in mainstream compression techniques such as JPEG and MP3, where JPEG uses discrete cosine basis and wavelet domain and MP3 is more compatible with modified discrete cosine transformation (MDCT) and Fourier transform [26].

In this thesis, we will highlight the complexity and orientation of the geometry, as well as the frequency and the type of RCS calculation (i.e. monostatic or multi-static), are all viable factors that are needed to be considered before selecting an appropriate transformation domain. Fortunately, empirical results show that CS works across a wide range of numerical methods such as the method of moments (MoM), physical optics (PO) and multilevel fast multipole (MLFMM). As most CS papers in the literature have a heavy emphasis on image signals, very few, if any, have shown detailed analyses of electromagnetic signals, the choices of transformation domain and reconstruction methods.

Previously, researchers [5][17][27] utilized DCT, FFT and Hermite transformation domains for RCS signals. [15] and [9] have compared, empirically, the reconstruction error of each domain above on a specific model. However, signals that appear to be sparse when expanded by certain transformation basis from a specific geometry model may not preserve the same sparsity when the same model is used, but with a different orientation, geometry model or frequency. Many natural image signals remain sparse or highly compressible in the same transformation domain (wavelet domain being the most popular choice) across a wide range of images of the same category.

2.6.1 Hermite Transform Domain

Hermite function, as an Eigen function of Fourier transform, plays an important role in many data compression tasks. Although data such as digital images, which are sparse in the Fourier transform domain, do not normally have sparse representations in Hermite transform domain, it is popularly

used in various applications such as ultra-high band communication channels and electrocardiogram (ECG) data [28].

As shown in [28], Hermite transform outperforms Fourier transform in certain types of signals that resemble QRS complexes. The inverse Hermite matrix of size M × N can be represented as

$$\boldsymbol{\psi} = \begin{bmatrix} \psi_0(0) & \psi_1(0) & \dots & \psi_{N-1}(0) \\ \psi_0(1) & \psi_1(1) & \cdots & \psi_{N-1}(1) \\ \vdots & \vdots & \vdots & \vdots \\ \psi_0(M-1) & \psi_1(M-1) & \dots & \psi_{N-1}(M-1) \end{bmatrix}, \tag{2-7}$$

and the direct Hermite transform matrix $\boldsymbol{H}$ is:

$$\boldsymbol{H} = \begin{bmatrix} \frac{\tau_0(0)}{\tau_{N-1}(0)} & \frac{\tau_0(1)}{\tau_{N-1}(1)} & \dots & \frac{\tau_0(M-1)}{(\tau_{N-1}(M-1))^2} \\ \frac{\tau_1(0)}{(\tau_{N-1}(0))^2} & \frac{\tau_1(1)}{(\tau_{N-1}(1))^2} & \cdots & \frac{\tau_1(M-1)}{(\tau_{N-1}(M-1))^2} \\ \vdots & \vdots & \vdots & \vdots \\ \frac{\tau_{N-1}(0)}{(\tau_{N-1}(0))^2} & \frac{\tau_{N-1}(1)}{(\tau_{N-1}(1))^2} & \dots & \frac{\tau_{N-1}(M-1)}{(\tau_{N-1}(M-1))^2} \end{bmatrix} \tag{2-8}$$

Under the context of CS, substituting the inverse Hermite matrix $\boldsymbol{\psi}$ to (1) gives:

$$\begin{bmatrix} x(0) \\ x(1) \\ \cdots \\ x(N-1) \end{bmatrix} = \begin{bmatrix} \psi_0(0) & \psi_1(0) & \dots & \psi_{N-1}(0) \\ \psi_0(1) & \psi_1(1) & \cdots & \psi_{N-1}(1) \\ \vdots & \vdots & \vdots & \vdots \\ \psi_0(M-1) & \psi_1(M-1) & \dots & \psi_{N-1}(M-1) \end{bmatrix} \cdot \begin{bmatrix} s(0) \\ s(1) \\ \cdots \\ s(N-1) \end{bmatrix} \tag{2-9}$$

where $\boldsymbol{x}$ represents the full signal and $\boldsymbol{s}$ represents the coefficients in Hermite transform domain. In reality, the Hermite transform matrix is much harder to implement than DFT and DCT. As the signal length increases, the polynomial degree and computation time increase drastically [28] Empirical results have shown that HT has the best performance for the parts of data that resemble bell-distribution, in which case the HT outperforms FFT. On the other hand, when the local behaviour of a signal does not resemble bell-distribution, the performance deteriorates.

2.6.2 Discrete Fourier Transform Domain

Fourier Transform conveniently captures a wide range of sinusoids or a superposition of sinusoids and transforms the signals from the time domain into the frequency domain. If the sinusoidal signals appear to be smooth with no disconnection, a sparse representation in the form of delta function can be obtained. Since real-life signals mostly have finite length, this thesis focuses on the discrete Fourier transform (DFT). A superposition of K sinusoids can be represented as:

$$X[n] = \sum_{k=0}^{K-1} a_k e^{-\frac{j2\pi}{K}nk} \tag{2-10}$$

where X[n] is the DFT transform of the sequence a_k and $0 \ll n \ll K-1$.
Fortunately, DFT can be easily expressed as a DFT matrix, which can be used as a dictionary or transformation matrix $\boldsymbol{\psi}$ [2]:

$$\begin{bmatrix} X(0) \\ X(1) \\ \vdots \\ X(N-1) \end{bmatrix} = \begin{bmatrix} 1 & 1 & 1 & 1 & 1 \\ 1 & W & W^2 & W^3 & W^{N-1} \\ 1 & W^2 & W^4 & W^6 & W^{N-2} \\ \vdots & \vdots & \vdots & \vdots & \vdots \\ 1 & W^{N-1} & W^{N-2} & W^{N-3} & W \end{bmatrix} \begin{bmatrix} a(0) \\ a(1) \\ \vdots \\ a(N-1) \end{bmatrix} \tag{2-11}$$

2.6.3 Discrete Cosine Transform

The Discrete Cosine transform is similar to the discrete Fourier transform that transforms signals from spatial/time domain to the frequency domain. However, while DFT is complex-valued, DCT is real-valued.

A 1D N-input DCT can be defined as the following equation:

$$\boldsymbol{X}(n) = \left(\frac{2}{N}\right)^{\frac{1}{2}N-1} \sum_{i=0}^{N-1} a(i) \cos\left(\frac{\pi(2n+1)k}{2N}\right), k = 0,1,\dots,N-1 \tag{2-12}$$

In fact, the DCT and be obtained from DFT by mirroring an original N given samples into 2N samples which perform better than DFT for certain scenarios where sharp discontinuities are caused by high-frequency segments[28].

All three transformation methods discussed above can be conveniently pre-calculated and stored as transformation matrices (or dictionaries). The functions do not change as signals change but the dimensions. However, the Hermite transformation matrix is substantially more computationally complex to calculate than the DCT and the DFT matrices.

2.7 Conclusion

In this chapter, the theory of Compressive Sensing, along with its mathematical foundation, was discussed. The essential fundamentals for CS-based application were introduced, including signal sparsity and the choice of the measurement matrix and transformation bases. In order to apply compressive sensing, the signal of interest must be sparse or highly compressible. Fortunately, many natural or synthetic signals can be found compressible in a suitable transformation basis, with the Hermite Polynomial, Discrete Fourier Transform and Discrete Cosine Transform being the most popular options for CS-based CEM applications. Finally, an incoherent measurement matrix that satisfies Restricted Isometry Property safeguards a high probability of success for signal reconstruction for CS applications. The next chapter focuses on the CS-based approaches for efficient RCS computation.

Chapter 3 CS for Radar Cross Section Computation

Although substantial studies on CS as a compression technique for digital imaging applications have been carried out, very few have extended the magic of CS to CEM applications. Thanks to recent advances in EM applications using compressive sensing [10][7], attentions have been brought to the possibility of utilizing CS for improving the efficiency of CEM applications. Compression techniques were developed to save storage of images with various quality standard. This chapter focuses on the proper implementation of CS-based techniques for improving the efficiency of computational EM problems, especially for the prediction of radar cross-section (RCS).

In the physical world, RCS measures the target's size and ability to reflect radar signal power in the direction of the radar receiver. In the case of monostatic RCS prediction, the transmitter and the receiver are located in the same direction. The prediction of RCS measurement is significant for high-performance radar and stealth objects designs. The equation of RCS, denoted by $\boldsymbol{E}$, is commonly known as:

$$\boldsymbol{E} = \lim_{r\to\infty} \frac{4\pi r^2 |\boldsymbol{E_s}|^2}{|\boldsymbol{E_i}|^2} \tag{3-1}$$

where r is the distance between the receiver and the target, and E_s and E_i represent the scattered and incident electric fields, respectively.

Under the CEM context, an inverse scattering problem or RCS computation problem, or EM scattering problem is to reconstruct certain physical, electrical or geometric characteristics of a given object from electric fields measurement when illuminated by some incident waves from certain directions [29]. In this thesis, the simulated RCS data are regarded as a vector, represented by the symbol $\boldsymbol{E}$, and referred to as a "signal" due to the fact that CS is mostly used under the signal processing context.

It is of high computational cost for RCS modelling and simulation for electrically large objects, where the object's dimensions are large compared to the wavelength of the incident wave. The past decades have seen a race in finding an efficient and effective solution for RCS computation. Asymptotic methods such as physical optics (PO) and Geometry Theory Diffraction (GTD) methods are capable of high-frequency RCS computation, but their accuracy is geometry-dependent[14]. A numerical method such as the Method of Moments is a full-wave analysis and can be applied to arbitrary geometries [6]. Unlike the asymptotic methods, the full-wave analysis has a high demand for computational resources. The fundamental idea behind CS for RCS simulation is to reduce a certain number of incident sources/transmitters during the pre-process and reconstruct the full signal at a later stage.

The CS-based technique significantly improves computational efficiency and is, theoretically, applicable to both numerical and asymptotic methods.

There are two different CS approaches for solving EM scattering problems in the literature. 1) current approach: Since the current calculation is inevitable in solving scattering problems, this method acquires under-sampled currents and later reconstruct them to save computational time. This is especially effective in some numerical methods such as the Method of Moments (MoM), in which the matrix equation imposes challenging computational cost in each iteration. 2) far-zone electric fields approach [15]: the compressed scattered and incident fields of a target is directly acquired from a random subset of the original incident angles for each unknown surface of the target and reconstructed to compute RCS.

The first method iteratively reconstructs currents across all angles from each unknown. Therefore, greedy methods, such as Orthogonal Matching Pursuit (OMP), are often used to minimize the reconstruction run-time of each iteration. The second method, which utilizes asymptotic EM solvers, only requires one-time reconstruction of the scattered field across all incident angles, thus offers faster computational speed over the first method. Also, it allows greater leeway for selecting an algorithm that provides improved reconstruction accuracy because the one-time reconstruction speed is negligible, although such an algorithm may not guarantee the fastest signal reconstruction.

3.1 Literature Review

Existing studies that combine Compressive Sensing with commercial EM modelling software have improved the efficiency of RCS calculation of simple targets at a very-high frequency (VHF) and low-end of Ultra-high frequency (UHF) [10] proposed *in situ* Compressive Sensing that first exploited Compressive Sensing framework in solving inverse scattering problems in a complex propagation medium.

In [10], an assessed Discrete Cosine Transformation using the established In Situ CS algorithm was proven more efficient than industry-accepted FEKO EM modelling software using various numerical methods such as Method of Moments and Multi-level Fast Multipole Method. [30] combined CS with MoM for 2D monostatic scattering (or backscattering) problems using Hermite polynomial as the basis functions for sparse representation of induced currents.

In [30], CS, in conjunction with MoM, was used to efficiently calculate monostatic scattering problems of 2D generic objects by introducing a new set of incident source. Although no specific reasons were given for the choice of transformation basis, Hermite polynomials were used as the basis functions.

In [9], an extended CS-MoM approach was developed to improve the efficiency of RCS prediction of 3D generic objects using a Fourier basis. In both [9] and [10], the authors developed a CS algorithm on Fortran because of its popularity and comparability in numeric and scientific computing, while other researchers also attempted to simulate RCS of generic objects using CS developed on MATLAB [30].

In the above papers, Compressive Sensing was used to resolving the unwieldy MoM matrix equation, which can be computationally expensive. However, for an electrically large object – that is when the wavelength is very small, and the conducting surface is flat with infinite extent, it is common to use an asymptotic method such as PO and GTD for their superior efficiency over numerical methods. Since inversion matrices, such as the MoM matrix, do not exist in asymptotic methods such as PO, CS cannot simply improve the speed for current calculation, although PO is a current-based method *per se*. This inspired researchers to integrate CS into a different stage of

inverse scattering problems for calculations using asymptotic methods. Naturally, the most straightforward approach is to exploit the scattered fields/RCS data for inverse scattering problems.

In [31], CS was applied to scattered fields of scaled generic objects using the PO method. However, the RCS pattern was only recovered for a small angular section of the original data.

As the demand for combining CS with commercial software has been increasing, in a recent study, [15] combined CS with a commercial EM modelling software FEKO for solving multi-static 3D scattering problems using MLFMA numerical method. Many industry-standard EM modelling software like FEKO and newFASANT allow the users to effectively import user-defined data and export simulation results with a convenient interface. Therefore, it is highly feasible to combine a CS algorithm developed in-house with EM solvers embedded in commercial-available software. Note that the commercial-available software must meet industry standards and preserves the same features, such as parallel computing when combined with an external program where compressive sensing is implemented. However, extra measures are often required to take full advantage of the commercial-available software. For example, FEKO uses the current solution from the previous angle to predict the next angle using phase correction to minimize the number of iterations for a linear set of excitations.

As discussed in [15], the Fast Fourier transform can be the sparest basis for the CS-based application. Although the choice of transformation basis varies for different CS techniques, researchers have been rather consistent with the reconstruction method, the Orthogonal Matching Pursuit.

In fact, most studies in the literature, including [9], [15], [31], and [30], relied on the OMP algorithm for signal reconstruction. However, most papers failed to explain the advantages of the OMP algorithm and to exploit and compare with different reconstruction algorithms. In this thesis, the efficiency of OMP and its variants is scrutinized and compared against an Iterative Shrinkage Thresholding Algorithm (ISTA) – Sparse Reconstruction by Separable Approximation (SpaRSA) [27], which utilizes a more practical performance through a more versatile scalar parameter and

group-separable regularizer that are suitable for different functional regions, where specific regularizers (i.e. l_2 and l_1 norms) are preferred for optimum speed and accuracy [30].

3.1.1 CS-Current Approach

In general, CS-based approaches improve the computational speed by reducing the number of incident sources such a problem would normally require. Since the most computationally complex stage in the Method of Moments is solving the matrix equation using matrix inversion technique, CS-current approach is mainly used to speed up the calculation of the MoM matrix equation. While it is possible to combine the CS-current approach with asymptotic methods, the effectiveness of the approach tends to be less impressive than those combined with MoM.

This section first explains the current approach for RCS problems. The following equation depicts the monostatic scattered fields from an angle θ[18]:

$$\boldsymbol{E_s}(\theta) = -ik\eta \frac{\exp(ik\rho_0)}{4\pi\rho_0} \hat{k}_{scat} \times \hat{k}_{scat} \times \int_s \exp\left(-ik\rho' \cdot \hat{k}_{scat}\right) J(\rho', \theta) ds' \quad (3\text{-}2)$$

where ρ_0 represents the distance between observation and original points, $\hat{k}$ is the unit vector.

Generally, the far-zone scattered electric field $\boldsymbol{E}$ due to the induced current $\boldsymbol{J}(\rho', \theta i)$ can be solved by the so-called Electric Field Integral Equation (EFIE). $\boldsymbol{J}$ is computed as follows:

$$\boldsymbol{J}(\rho', \theta_i) = \boldsymbol{I}_i(\theta_i)\boldsymbol{P}_i(\rho') \quad (3\text{-}3)$$

where $\boldsymbol{P_i}$ is the basis expansion function, and $\boldsymbol{I}_i$ is the unknown basis expansion coefficient, i = 1, 2, ..., N is the number of incident angles, and ρ' and θ_i represent the source position and the incident angles, respectively. MoM reduces EFIE to a complex matrix equation in which we can compute the current vector $\boldsymbol{I}$ to calculate the far-zone scattered electric fields.

$$\mathbf{Z}\boldsymbol{I}_k(\theta_i) = \boldsymbol{V}_k(\theta_i) \quad (3\text{-}4)$$

where $\boldsymbol{Z}$ and $\boldsymbol{V}$ represent the respective impedance and excitation matrices, and k = 1, 2, ..., n is the number of unknowns. Note that the term ”unknowns” is essentially the number of basis expansion coefficients, which is generally larger than the number of meshes [30]. We also refer to these meshes as patches as they are essentially part of the object’s surfaces. For every scattering angle, a distinct value of $\boldsymbol{V}$ is calculated at each mesh of the target. Traditionally, excitation from all incident angles ($\boldsymbol{\theta}_{N\times 1}$) is taken into account resulting in a full $n \times N$ matrix, $\boldsymbol{V}$. By applying CS, we introduce a new set of incident sources located at the incident angles, $\boldsymbol{\theta}_{\boldsymbol{CS}}$, which are selected by an identically distributed (i.i.d) random matrix $\boldsymbol{\Phi}_{\mathrm{M\times N}}$.

In the signal processing perspective, this process symbolizes the compression capability of compressive sensing.

$$\boldsymbol{\theta}_{\boldsymbol{CS}_{M\times 1}} = \boldsymbol{\Phi}_{M\times N}\boldsymbol{\theta}_{N\times 1} \tag{3-5}$$

To understand the dynamics of equation (3-5), one can visualize the original incident angles and the compressed incident angles from a given cutting plane in the angular coordinate.

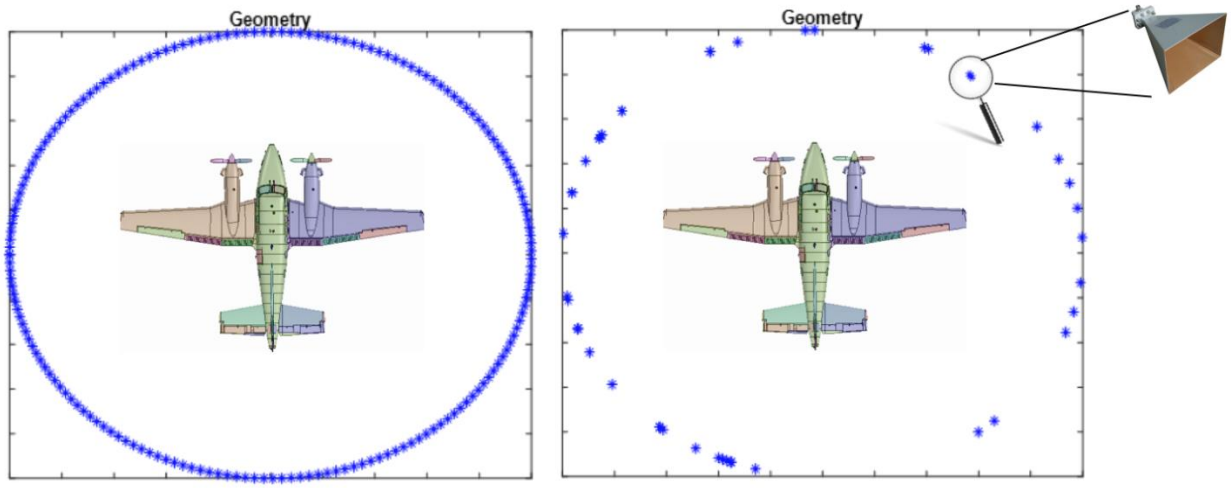

Figure 5 - Original Incident Angles vs. Compressed

As shown in Figure 5, the target (i.e. an aircraft) is observed at every 1 degree from $0^\circ < \theta < 360^\circ$ for a total of 361 incident angles. The compressed angles are randomly distributed across the $0^\circ < \theta < 360^\circ$ for a total of $\mathrm{M} \ll 361$ angles [32].

The choice of sensing matrix $\boldsymbol{\Phi}$ determines whether the procedure is a traditional sense of CS in which all atoms in $\boldsymbol{\Phi}$ are randomly selected (i.e. Gaussian random matrix) or structured. As

addressed in the previous section, a sparse or compressible signal has a concise representation in some transformation basis $\boldsymbol{\Psi}$.

Therefore, the current on the k^{th} mesh over all angular ranges (θ = 1, 2,..., N) where the original sources are distributed can be represented in a sparse domain:

$$|I_k(\theta_1) \quad I_k(\theta_2) \quad \cdots \quad I_k(\theta_3)| = \boldsymbol{\Psi}_{N\times N} \begin{vmatrix} y_k(\theta_1) \\ y_k(\theta_2) \\ \vdots \\ y_k(\theta_N) \end{vmatrix} \tag{3-6}$$

where $\boldsymbol{y}$ is the measurement vector of the original current.

Since $\boldsymbol{y}$ is sparse and only have a few dominant coefficients, we can construct the new currents with respect to the sensing matrix.

$$\boldsymbol{I}_{CS_{M\times 1}} = \boldsymbol{\Phi}_{M\times N}\boldsymbol{\Psi}_{N\times N} \begin{vmatrix} y_k(\theta_1) \\ y_k(\theta_2) \\ \vdots \\ y_k(\theta_N) \end{vmatrix} \tag{3-7}$$

where $\boldsymbol{I}_{CS}$ can be computed from the MoM matrix equation $\boldsymbol{Z}_{N\times N}\boldsymbol{I}_{CS_{M\times N}} = \boldsymbol{V}_{CS_{M\times N}}$. .

The measurements $\boldsymbol{y}$ of the induced currents can be reconstructed from equation (3-7) by greedy or convex optimization methods, which will be addressed in detail in the reconstruction algorithm section.

3.1.2 Combine CS-Current with EM Modelling Software

The CS-Current approach can be easily combined with commercial-off-the-shelf electromagnetics simulation software such as FEKO and newFASANT. The procedure can be decomposed into three major sections: pre-processing, MoM solver and post-processing as can be seen in Figure 6.

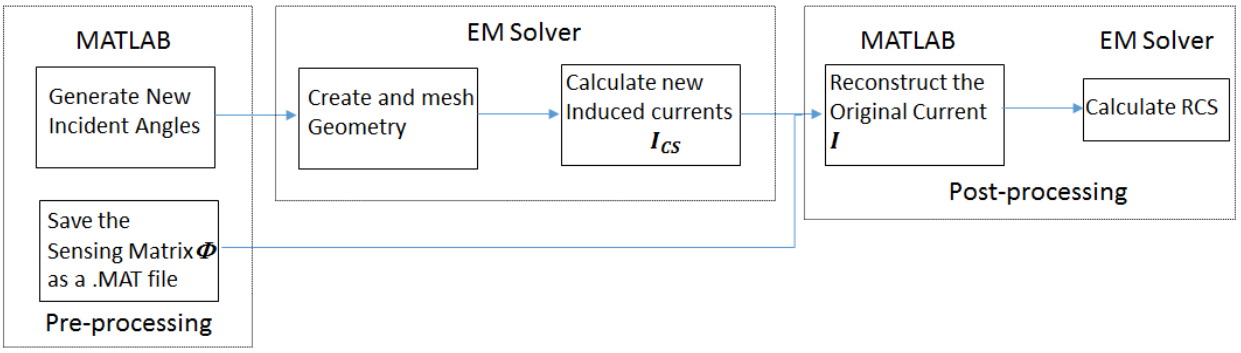

Figure 6 - MATLAB-Based CS-Current Approach Combined with Commercial Software

1. Use MATLAB to generate new incident angles where the incident sources are located, and save the sensing matrix $\boldsymbol{\Phi}$ for later reference;

2. import the new incident angles to commercial EM solver; use the commercial software to create and mesh the geometry and calculate the currents concerning the given incident sources

3. Export the ICS in ASCII (FEKO) or Binary (newFASANT) format; use a reconstruction method to recover the original currents (or basis expansion coefficients) $\boldsymbol{I}$; Import the reconstructed $\boldsymbol{I}$ back to the EM solver for final RCS calculation

The post-process requires prior knowledge of the sensing matrix $\boldsymbol{\Phi}$ for appropriate signal reconstruction. Therefore, one shall only generate $\boldsymbol{\Phi}$ once during the pre-process and reuse it for all future processes. Despite the seemingly long procedure, most of the operations described above can be automated in both MATLAB and the designated EM solver. For instance, since the current file format is fixed and often well documented in user manuals, one can simply create a MATLAB function for file conversion.

3.2 CS-RCS Approach

This thesis proposes a different approach than the traditional current approach described in the previous section. Instead of compressing the surface current on every unknown (or mesh), the proposed CS-RCS approach 1) compresses RCS signal across all directions, 2) directly uses the under-sampled RCS generated by the selected EM solver for efficient signal reconstruction. Fundamentally, both CS-RCS and CS-current improves computation run-time by reducing the

number of excitations required for the simulation. They both compress and reconstruct signals calculated using EM field solver by utilizing their sparse representation in a transformation domain. However, the CS-Current method is only effective in MoM by reducing the computational complexity of the MoM matrix equation. Conceptually, the CS-RCS approach proposed here is close to the far-zone scattered-field approach addressed in [15]. However, [15] extracted the real and imaginary parts of the far-zone electric fields from FEKO but did not directly use RCS as the signal of interest. In contrast to CS-RCS, the CS-Electric Fields approach acquires under-sampled scattered and incident electric fields from $M \ll N$ randomly selected directions, which are then used to compute the under-sampled RCS. This allows one to skip the redundant step of having to recover the currents of hundreds of thousands of unknowns from all directions. However, in order to calculate RCS, the CS-Electric Fields approach requires reconstruction of both the far-zone scattered fields and the incident fields. While the former is compressible in Fourier basis, a sparse/compressible representation cannot be found for the latter. As a result, the under-sampled incident fields cannot be reconstructed properly under the CS framework. Although incident fields can often be a fraction of magnitude of the scattered fields, its impact on the overall RCS reconstruction accuracy cannot be neglected. Chapter 4 will show that the reconstruction of RCS as the signal of interest yields higher accuracy than the reconstruction of the complex, real or imaginary part of scattered fields.

The CS-RCS approach has the following advantages over the aforementioned current approach:

1. Reduced computational complexity by directly recovering the RCS instead of currents of each unknown.
2. Instead of having to substitute the recovered currents back into the commercial EM software, the RCS can be conveniently computed using MATLAB.

Consider the frequency-dependent RCS data across N incident angles as a complex-valued and one-dimensional discrete-time signal $\boldsymbol{E}$ with length N. If $\boldsymbol{E}$ has a sparse representation in a basis of NxN matrix $\boldsymbol{\Psi}_{N\times N}$, the signal can be represented as:

$$\boldsymbol{E} = \sum_{i,j=1}^{N} s_i \psi_{i,j} \quad or \quad \boldsymbol{E}_{N\times 1} = \boldsymbol{\Psi}_{N\times N}\mathbf{s}_{N\times 1} \tag{3-8}$$

where $\boldsymbol{s}$ is the Nx1 column vector that corresponds to the coefficients of the signal in $\boldsymbol{\Psi}$ domain. Note that $\boldsymbol{s}$ represents the RCS signal in $\boldsymbol{\Psi}$ domain while $\boldsymbol{E}$ represents the signal in the spatial domain. The signal $\boldsymbol{E}$ is so-called "K-Sparse" if it has at most K non-zero entries. In reality, scattering signals can be found highly compressible in suitable transformation domain, in which a scattering signal consists of a few large coefficients and many small coefficients in vector $\boldsymbol{s}$. Similar to the CS current approach, the compressed incident angles are calculated using equation (3-5).

This approach is applicable to the MoM method as described in equation (3-2), where the under-sampled currents acquired from M randomly selected directions $\boldsymbol{\theta}_{\boldsymbol{CS}_{M\times 1}} = \boldsymbol{\Phi}_{M\times N}\boldsymbol{\theta}_{N\times 1}$ can be calculated using a pseudo-inverse $\boldsymbol{Z}_{n\times n}\boldsymbol{I}_{M\times n} = \boldsymbol{V}_{M\times n}$. Also, CS-RCS can be applied to variations of MoM (e.g. MLFMM) and other asymptotic EM methods, such as physical optics. In contrast to MoM, PO avoids the iterative and costly inverse matrix equations and is inherently computationally less complex than MoM. While numerical methods accurately calculate the scattering data given necessary computation power, PO provides satisfactory RCS approximation of electrically-large objects, such as objects that are tens of meters long in each dimension at microwave frequencies. Similarly, the physical optics (PO) currents on perfect electric conductor (PEC) surfaces can be represented as [11][14]:

$$J = 2\hat{n} \times H^i \tag{3-9}$$

where i is the incident angle and $\hat{n}$ denotes the normal unit vector.

3.2.1 Combine CS-RCS Approach with EM Modelling Software

This section provides detailed procedures for the CS-RCS approach. The proposed CS can be applied to arbitrary EM numerical solvers such as asymptotic and numerical algorithms. Also, one can easily apply the CS-based method to various commercial-off-the-shelf electromagnetics simulation software such as newFASANT and FEKO. However, this thesis has a focus on the newFASANT software and its native PO algorithm as the EM solver. The process can be decomposed into three major sections: pre-processing, EM numerical solver and post-processing. MATLAB is used at both the pre-processing and the post-processing stages.

1. Use MATLAB to generate new incident angles where the incident source are located, and save the sensing matrix $\boldsymbol{\Phi}$ for later reference;

2. Import the new incident angles to a commercial EM solver; use the commercial software to create and mesh the geometry and calculate the RCS concerning the given incident sources;

3. Export the E in ASCII format; use a reconstruction method to recover the original RCS data;

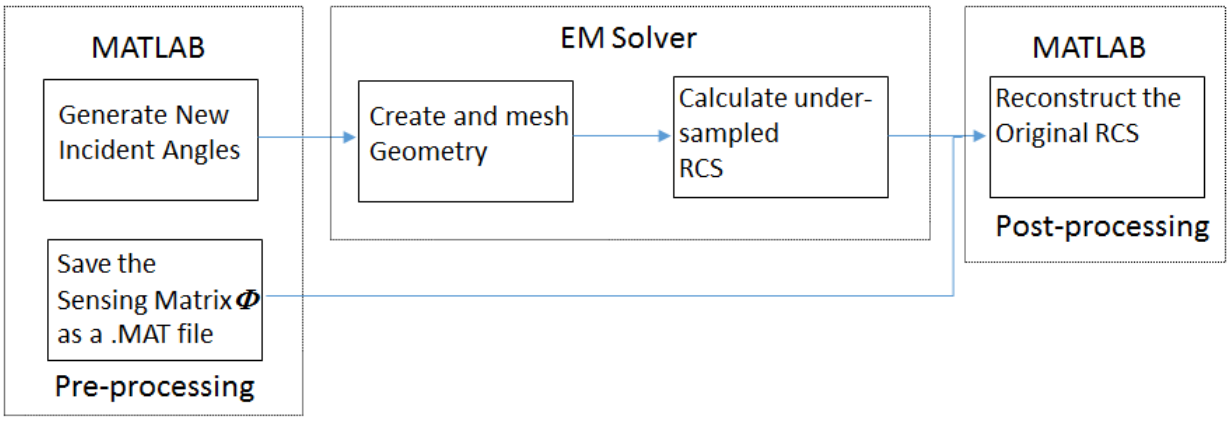

Figure 7 - MATLAB-Based CS-RCS Approach Combined with Commercial Software

The post-process requires prior knowledge of the sensing matrix $\boldsymbol{\Phi}$ for appropriate signal reconstruction. Therefore, one shall only generate $\boldsymbol{\Phi}$ once during the pre-process and reuse it for all future processes. Also, most of the operations described above can be automated in both MATLAB and the designated EM solver. Instead of having to reconstruct every iteration for every unknown (3120 iterations for a simple 4m by 4m plate at 300MHz), the CS-RCS approach only requires one-time reconstruction regardless of the number of unknowns.

3.3 Reconstruction Algorithms

A proper reconstruction algorithm extends the magic of compressive sensing in Computational Electromagnetics applications. Greedy methods such as matching pursuit and orthogonal matching pursuit offer fast recovery while convex optimizations such as Basic Pursuit are often more robust [33]. This section explains and compares different types of reconstruction algorithms. Most CS studies for CEM applications found in the technical literature did not compare the difference between different types of reconstruction algorithms. For compressive sensing, finding $\boldsymbol{y}$ from $\boldsymbol{s}$ and $\boldsymbol{A}$ can be seen as a compression problem because $\boldsymbol{y}$ is a sparse representation of the original

signal $\boldsymbol{s}$ in a transformation domain described by matrix $\boldsymbol{A}$. In contrary, finding the transformed representation $\boldsymbol{s}$ from $\boldsymbol{y}$ and $\boldsymbol{A}$ is called reconstruction or recovery. In RCS problems, for example, $\boldsymbol{s} \in \mathbb{R}^{\boldsymbol{N}}$ is the true unknown signal consists of Radar signature of a target from all directions under the Fourier basis, and $\boldsymbol{y} \in \mathbb{R}^{\boldsymbol{M}}$ represents the under-sampled Radar image acquired from a reduced number of directions. In these applications, the matrix $\boldsymbol{A} \in \mathbb{R}^{\boldsymbol{M} \times \boldsymbol{N}}$ acts as a two-dimensional convolution operator. Notice that $\boldsymbol{y}$ is often shown as a blurred image in image processing applications; it cannot be conveniently shown as a blurred Radar image in RCS applications.

Reconstruction or recovery algorithms are applied to recover signals compressed via CS procedures. Ideally, a sparse signal can be fully recovered with a high percentage by solving an $l1$ norm minimization problem [34]. Naturally, many real-life signals are not sparse in a strict sense but compressible in the respective transformation domains. Furthermore, some signals may be contaminated by noises of various forms. This section probes algorithms concerning CS signal recovery. Depending on the sparsity, type and noise level of the signal, the speed and effectiveness (or accuracy) of different reconstruction algorithms vary. Simulation results that provide the performance of different algorithms in terms of efficiency/accuracy are available in Chapter 4.

3.3.1 Convex Optimization

Mathematically, the main objective of an optimization problem is to find a global maximum, minimum, or simply "optimal," of an object function f_0 via the search of a certain set of variables $\boldsymbol{s} = s_1, \dots s_n$ ($\boldsymbol{s} \in R$) that satisfy the conditions defined by a constraint function f_i. In the convex optimization problem, the goal is to attain an optimal point from a convex function, which, geometrically, can be pictured as a bowl-shaped function. Also, the objective and constraint functions must all be convex functions.

$$\begin{aligned} & minimize\ (or\ min.) && f_0(s) \\ subject\ to\quad & f_i(s) \le 0, i = 1, \dots, m && h_i(s) = 0, i = 1, \dots, p \end{aligned} \tag{3-10}$$

Both linear programming problems and Least-squares problems that resemble the following form are common convex optimization problems

$$minimize\ (or\ min.) \qquad f_0(x) = \|As - y\|_2^2 \tag{3-11}$$

where $\boldsymbol{A} \in \mathbb{R}^{\boldsymbol{M}\times\boldsymbol{N}}$ and $\boldsymbol{s} \in \mathbb{R}^{\boldsymbol{N}}$, in this section, inherit the same notations and definitions from equation (2-2) in Chapter 2. Note that $\boldsymbol{s}$ is not the original signal but the representation of the original signal in a transformation basis.

3.3.1.1 Basic Pursuit

In the cases where signal $\boldsymbol{s}$ in equation (2-2) is sparse in the transformation domain, the current/electric fields can be reconstructed by solving an l_p minimization problem:

$$min\|x\|_p\ subject\ to\ \boldsymbol{y} = \boldsymbol{As} \tag{3-12}$$

When p = 0, reconstructing the k-sparse vector $\boldsymbol{s}$ from its measurement $\boldsymbol{y}$ is N-P hard and very unpractical because of the total choice of combinations or subsets of $\binom{N}{k}$ can be very large. l_0 norm counts the total number of nonzero coefficients. Similarly, it is a non-convex problem and N-P hard for 0 < p < 1; p = 1, as shown in equation (3-13), provides closest convex optimization to approximate the aforementioned non-convex problems.

$$min\|x\|_1\ subject\ to\ \boldsymbol{y} = \boldsymbol{As} \tag{3-13}$$

While l_2 norm, also a popular choice among convex optimization methods, often fails to provide the sparest solution. This problem, which is generally known as l_1-norm minimization or a convex relaxation in the literature, can be reformulated as:

$$min\|\boldsymbol{As} - \boldsymbol{y}\|_2\ subject\ to\ \|\boldsymbol{s}\|_1 \leq K \tag{3-14}$$

where K is the sparsity of the signal. When $\boldsymbol{s}$ is very sparse, and the measurement matrix $\boldsymbol{A}$ is orthonormal in a strict sense, there is a high chance that excellent recovery can be achieved using l_1-norm minimization.

Furthermore, l_1-norm based algorithms that accommodate measurement noise and digitization errors are called Basis Pursuit de-noising (BPDN)[21]:

$$\frac{1}{2}\|\boldsymbol{y}-\boldsymbol{A}\boldsymbol{s}\|_2^2+\lambda\|\boldsymbol{s}\|_1 \text{ for } \lambda \geq 0 \tag{3-15}$$

In the statistics literature, the least absolute shrinkage and selection operator (LASSO) is used instead of BPDN. However, the difference between LASSO, BPDN and quadratically constrained BP are subtle.

3.3.1.2 Sparse Reconstruction by Separable Approximation

SpaRSA is a framework of Iterative Shrinkage-Thresholding Algorithm (ISTA) that solves the following optimization problem [35]:

$$\min_{x\in\mathcal{R}^n}\phi(s) \coloneqq f(s)+\tau c(s) \tag{3-16}$$

where $f(s)$ is a smooth function, $c(s)$ is possibly a convex non-smooth regulizer, and τ is a regularization parameter that controls the tradeoff between noise sensitivity and the measurement fidelity. In contrast to other reconstruction algorithms, for each iteration, ISTA conducts matrix-vector multiplication $\boldsymbol{A}^T\boldsymbol{A}$, the Hessian of $\|y-As\|_2^2$, and $\boldsymbol{A}^T(\boldsymbol{A}s^k-\boldsymbol{y})$, which is the gradient (Δf) of $\frac{1}{2}\|\boldsymbol{y}-\boldsymbol{A}\boldsymbol{s}\|_2^2$ [36]. For CS applications where FFT and wavelets are used, the gradient search is computationally inexpensive for the matrix-vector multiplication (matrix $\boldsymbol{A}$ and its transpose $\boldsymbol{A}^T$), which tends to be the most costly procedure in ISTA [36]. Therefore, ISTA is a simpler and more efficient alternative for solving BPDN problems, especially for applications that

involve large scale and dense matrix data. When $\tau = 0$, the problem becomes a gradient descent line search [37].

The general algorithm for ISTA is the following:

$$s_{k+1} = \mathcal{T}_{\lambda t}(s_k - 2\boldsymbol{A}) \tag{3-17}$$

In compressive sensing and other signal processing applications, this solves the famous l_2-l_1 problem – the BPDN problem [37].

$$s_{k+1} = \mathcal{T}_{\lambda t}(s_k - 2tA^T(\boldsymbol{A}s_k - \mathrm{y})) \tag{3-18}$$

where t is the step size and $\mathcal{T}_\alpha$ is the shrinkage operator.

As the purpose of compressive sensing is to speed up the computation runtime, SpaRSA, as proposed in [27], solves the optimization problem (3-16) using less conservative scalar parameter α and an accelerated approach compared to the traditional ISTA [27]. Also, SpaRSA is more effective than ISTA in CS since ISTA relies on the bonding of $\boldsymbol{A}^T\boldsymbol{A}$ by a diagonal such as $\boldsymbol{D} - \boldsymbol{A}^T\boldsymbol{A}$. This bound is tight only when the sensing matrix $\boldsymbol{\Phi}$ resembles a square matrix. However, in CS, such bond is loose, as $\boldsymbol{\Phi}$ has much fewer rows than columns. Therefore, this thesis uses SpaRSA combined with the CS-RCS approach to solve RCS computation problems.

Generally, SpaRSA solves the following problem at each iteration [27]:

$$s^{t+1} \in arg\min_z (\boldsymbol{z} - \boldsymbol{s}^t)^T \nabla f(s^t) + \frac{\alpha_t}{2}\|\boldsymbol{z} - \boldsymbol{s}^t\|_2^2 + \tau c(z) \tag{3-19}$$

for a sequence of iteration where t = 0, 1, … for some $\alpha_t \in \mathbb{R}^{\boldsymbol{N}}$ and ∇f is one of the most inexpensive ways to solve equation (3-16). $\boldsymbol{s}$ is the original signal and $\boldsymbol{z}$ is the possibly noise-corrupted observation of $\boldsymbol{s}$. There are several variations of SpaRSA depends on how α_t is selected. For CEM application, this thesis utilizes the Barzilai – Borwein (BB), which is a spectral non-

monotone method where the objective function does not decrease at every iteration[38]. The SpaRSA algorithm, according to [27], can be described as summarized in Table 1.

Similar to other gradient-based and iterative thresholding algorithms, SpaRSA benefits greatly from a "warm starting point." SpaRSA utilizes the solution of equation (3-16) from the previous interaction for a given value of τ to initialize the algorithm in solving equation (3-16) for a nearby value of τ [38]. By utilizing the solution from the first run, the second run requires 1) fewer iterations than the first run and, 2) much fewer iterations than if it were initialized at zero because the first run solution is closer to the second run solution.

Table 1- SpaRSA Algorithm

Input:
Factor $\eta > 1$
Scalar parameter $[\alpha_{min}, \alpha_{max}] \in (0, \infty)$
Initialize:
Iteration counter t = 0
Initial guess x^0
Procedure:

1. Choose $\alpha_0 \in [\alpha_{min}, \alpha_{max}]$ using the BB method:

   Let $\alpha_0 = arg \min_{\alpha} \|\alpha(s^t - s^{t-1}) - r^t\|_2^2$ where $r^t \approx \alpha(s^t - s^{t-1})$ in the least square sense

2. Set $\alpha = \eta^k \alpha_0$ where $k \geq 0$ is the closest integer to 0 so that

   $\phi(s^{t+1}) \leq \max_{i=[t-M,t]} \phi(s^i) - \sigma\, \alpha_t \|s^{t+1} - s^t\|^2$, where $\sigma \in (0,1)$

3. If $s^{t+1} = s^t$, stop
4. $t = t + 1$
5. Repeat

For SpaRSA algorithm, the runtime significantly degrades when τ tends to be small. In a noisy case, a larger τ offers better noise reduction; however, this inevitably creates more loss of low-contrast features[39].

As suggested in [27], [36], and [38], the convergence of an l_1-regularized Least-Square problem happens for a regularization parameter with a finite value

$$\tau = \tau_{\max} \geq \|2\mathbf{A}^{\mathrm{T}}\mathbf{y}\|_{\infty} \tag{3-20}$$

Note that, for a noiseless CS application, as τ decreases, the solution has a high possibility to be sparse, but it also poses a threat to deteriorate the algorithm's performance with drastically slower runtime. So, the runtime significantly degrades when τ tends to be small. On the contrary, although a larger τ offers faster runtime and better noise reduction than a smaller τ, it inevitably creates more loss of low-contrast features [39].

3.3.2 Greedy methods

Iterative greedy algorithms are among one of the most popular reconstruction methods for compressive sensing applications thanks to its fast computational speed. In comparison with the l_1-norm based optimization algorithms, greedy methods are less computationally complex and more efficient in signal recovery at the expense of reconstruction accuracy, especially if the sparsity of the signal is low.

Surprisingly, OMP has been one of the most popular reconstruction algorithms for scattering signals recovery for compressive sensing based applications [17]. With its computationally efficient characteristics, the greedy method received attention in the current approach for solving scattering problems, where the currents of each unknown must be reconstructed often for tens of hundreds of iterations depend on the frequency. However, reconstruction methods have not been scrutinized for inverse scattering problems in the literature, and OMP has been repeatedly and continuously used in CS-based CEM applications without much of justification. In this thesis, through empirical results, we argue that OMP does not provide the best performance for scattering signal recovery despite its inherent speed advantage as a greedy method. Since the RCS approach conveniently requires only one-time reconstruction regardless of the observing frequency, the reconstruction time is negligible compared to RCS computation time.

OMP is evolved from Matching Pursuit (MP), discussed in [40], that aims to find a unique set of linear expansions of waveforms the solution of s for $\boldsymbol{y} = \boldsymbol{As}$, where $\boldsymbol{y}$ and $\boldsymbol{A}$ are known, by fixing the support of $\boldsymbol{s} \in \mathcal{R}^n$. By doing so, one can determine the zero or non-zero entry of $\boldsymbol{s}$. However, in contrast to MP, OMP includes an additional orthogonalization step that significantly improves runtime[17]. The nature of greedy methods, including MP, seeks approximate solution instead of a perfect solution to accelerate the optimization process.

OMP algorithm finds the strongest atom in the matrix $\boldsymbol{A}$ that contribute the most to $\boldsymbol{y}$. Then the algorithm determines the atom that contributes the second most to $\boldsymbol{y}$ from the residual. This process takes N iterations, where N represents the number of atoms in matrix $\boldsymbol{A}$. Geometrically, the residual is perpendicular to the contribution of the first selected basis [20].

Table 2 - Orthogonal Matching Pursuit Algorithm

Input:

- measurement matrix $\boldsymbol{A} \in \mathbb{R}^{\boldsymbol{M}\times\boldsymbol{N}}$
- measured vector $\boldsymbol{y} \in \mathbb{R}^{\boldsymbol{M}}$
- original K-sparse vector $\boldsymbol{s} \in \mathbb{R}^{\boldsymbol{N}}$

Initialization:

- residual r(0)=$\boldsymbol{y}$; estimated signal $\hat{s}(0) = 0$

Procedure:

1. for i=1,…,k
2. $\lambda(i) = argmax\ j = 1, \dots, N \left|\langle r(i-1), \phi_j \rangle\right|$
3. $\boldsymbol{A} = \left[\boldsymbol{A}(i-1)\ a_{\lambda(i)}\right]$
4. $x(i) = \ argmin\ \hat{s} \|y - \boldsymbol{A}(i)\hat{s}\|_2^2$
5. $\mathrm{r(i)} = \boldsymbol{y} - \boldsymbol{A}(i)s(i)$
6. end

Output:

- $Estimated\ \hat{s} \in \mathbb{R}^{\boldsymbol{N}}$
- $Residual\ r$

Step 4 of Table 2 finds the maximum correlation column of the sensing matrix with the residual and enables the OMP with superior runtime over MP.

Further advances in the OMP algorithm includes the Compressive Sensing Matching Pursuit (CoSaMP)[33] and the Regularized Orthonormal Matching Pursuit (ROMP)[41]. CoSaMP, as its name suggests, is claimed to be efficient in solving practical compressive sensing problems with more rigorous noise bounds[33]. In fact, CoSaMP [33] was inspired by ROMP, which established RIP on the basis of OMP to offer a regularized reconstruction for compressible and noisy signals [41].

Table 3 - Relative Performance of different reconstruction algorithms. K refers to the sparsity; m refers to the number of measurements; N refers to the original signal length

Lp Reconstruction	**CoSaMP**	**OMP**	**ROMP**	**Convex**
Optimal number of samples	Within *O*(KlogN)	Within *O*(KlogN)	>*O*(KlogN)	Within *O*(KlogN)
Stability	Compressible and noisy signal	Compressible signal	Compressible and noisy signal	Compressible and noisy signal
Running time	*O*(mN)	*O*(KmN)	*O*(KmN)	LP(N,m)

Table 3 depicts the performance of typical algorithms that solve a convex problem, greedy methods such as OMP, CoSaMP and ROMP. The optimal number of samples defines how many measurements the algorithm requires to reconstruct a K-sparse signal. The stability of an algorithm is whether the signal works with compressible but not sparse or noisy signals. LP(N,m) denotes the total cost of solving a linear problem with length N using m measurements [33].

3.4 RCS Convergence Algorithm

Intense research has been conducted to develop various reconstruction algorithms to fulfill the computational need of the ever-changing technology world. As described in the previous section,

different reconstruction methods have been developed and evolved to satisfy some unique aspects that different applications demand, whether they are accuracy, speed, signal-smoothing or noise-cancelling. Greedy methods provide paramount speed performance compared to most of the algorithms that solve a convex problem. However, Greedy methods, such as OMP, only yield accurate reconstruction results with some tolerance to noises when the reconstructed signal is sparse. Evolved from OMP, [41] proposed regularized OMP or ROMP that utilizes a more sophisticated selection rule and recovers compressible signal corrupted by noises. ISTA and gradient methods can solve a convex optimization problem efficiently and are computationally less complex than the traditional l_1-norm based optimization problem.

Truth be told, most reconstruction algorithms require *a prior* information, either on the signals' sparsity (i.e. the number of non-zero coefficients), measurement or both. For example, most greedy methods (e.g. OMP and its variants) and l_1-norm based algorithms require *a priori* knowledge of the sparsity of the signal in order for an accurate reconstruction. Unfortunately, the sparsity of scattering signals from CEM applications is unpredictable. There is an infinite number of objects, and each object may have different orientation, physical and electrical size, which all contribute to an unpredictable pattern of signal sparsity. However, most papers that study CS-based solution for efficient scattering problems failed to acknowledge the variety of reconstruction algorithms and their proper usage. For example, [9][15][16] use OMP reconstruction algorithm by default without specifying how the signal sparsity or the number of non-zero coefficients were determined. Besides, the number of measurements required to reconstruct a signal properly is hypothetical, although, as discussed in Chapter 2, a rough range of measurements for sparse signals, $M \geq cKlog(\frac{N}{K}) \ll N$, can be used for estimation[6].

SpaRSA, on the other hand, does not require *a priori* knowledge of signal sparsity. Instead, it requires the user to define a regularization parameter, which can be determined conveniently using equation (3-20). However, this does not immune SpaRSA from the fact that an appropriate number of measurements is required for an accurate reconstruction. Generally, this poses the following issues:

1. Not enough measurements resulting in inaccurate reconstruction

2. Too many measurements that affect the efficiency

As can be seen in Table 4, a MATLAB script is designed to find the minimal number of measurements that results in an accurate RCS reconstruction. Succinctly, the script accumulates the number of measurements for each iteration and compares the reconstructed RCS of the current iteration with the previous one. The number of measurements converges when the Frobenius norm between the RCS at the current iteration and the RCS at the previous iteration is smaller than a given threshold, ζ.

Table 4 - RCS Convergence Algorithm

Input:

- Transformation matrix $\boldsymbol{\Psi} \in \mathbb{R}^{N\times N}$
- Original signal length N

Initialization:

- Count n
- Initial measurement m $\ll N$
- Sensing matrix $\boldsymbol{\Phi} \in 0^{N\times N}$
- Threshold ζ

Procedure:

1. While $\mathrm{e} = \frac{\|\boldsymbol{RCS^{n-1}} - \boldsymbol{RCS^{n-2}}\|_F}{\|\boldsymbol{RCS^{n-2}}\|_F} \leq \zeta$
2. Let m random position in $\boldsymbol{\Phi}$ =1
3. Calculate RCS^n using
4. $m = m + 0.1N$
5. $n = n + 1$
6. return

If RIP and incoherence hold, a K sparse signal of length N is recoverable from m measurement with the following relationship with K and N: $m = O(K \log(\frac{N}{K})) \ll N$. The notation O characterize the growth rate of measurements according to the signal sparsity. It shows that even when the signal sparsity/compressibility decreases linearly, the number of measurement needed to recover the signal increases logarithmically, which is much slower than a linear increase. The initial guess m is a quarter of the signal length; this rule comes from empirical experiences addressed in [34][24]

under the condition that the signal is strictly sparse with incoherent measurement matrix and reconstructed by *l*1-minimization. In the case of RCS signals of complex targets, the signals are less-than-sparse that typically require more measurements. Therefore m initiates from $m = N/4$.

3.5 Conclusion

This chapter has a focus on applying CS to Computational Electromagnetics applications, especially for Radar Cross Section simulation. The conventional currents-based and electric-field-based CS approaches found in the open literature were reviewed in detail. The CS-RCS approach, which utilizes RCS signal as the signal of interest, was proposed to improve the speed of RCS calculation using commercial EM software. Finally, this chapter discusses an accelerated iterative thresholding algorithm – SpaRSA and provides a review of greedy algorithms. Through numerical results demonstrated in the next chapter, we argue that the SpaRSA algorithm has the potential to greatly improve the performance of CS-RCS approach.

Chapter 4 Numerical Results

This section provides numerical and simulation results to analyze the proposed CS-RCS approach, transformation bases and reconstruction algorithms using various objects of different levels of complexity. The conventional current and the electric field approaches were also reviewed and compared. Simulations of simple and generic objects were first conducted and compared for the proposed CS-RCS algorithm, and signals were recovered using various reconstruction algorithms mentioned in Chapter 3. Then, the proposed CS-RCS, combined with the SpaRSA reconstruction algorithm, was examined using a complex and electronically large target. All results were simulated using the newFASANT software combined with CS-based approaches (CS-Current and CS-RCS) implemented in a MATLAB program. In this thesis, we used the MATLAB-based OMP, CoSamP and BP algorithms from the open-source code – SparseLab developed by Donoho *et al.* from Stanford University [2].

One may notice that the complexity of the objects gradually increase, as the goal of the proposed algorithm is to improve the efficiency of real-life electronically large objects with potentially complex structure, such as a Canadian King Air aircraft. Previously, most studies on CS-based CEM applications focused on the lower end of the microwave frequencies. In this Chapter, both generic and complex targets were simulated using various frequencies ranging from the lower end of microwave frequencies (e.g. 400MHz) to the higher end of L band (e.g. 1-2GHz) frequencies that fall into the electronic warfare (EW) frequency of interest. Ultimately, this chapter analyzes and compares the performance, in terms of accuracy and efficiency, of a series of combinations of the bases and algorithms using CS-RCS frequencies. This section also looks into the relationship between the CS-RCS reconstruction accuracy and the RCS angular resolution (AR). AR is an inherent parameter of any radar imaging data. The angular resolution of RCS not only determines how much detail the radar image captures but also determines how smooth the simulated RCS signal is. Therefore, one may increase the angular resolution as a mitigator of spurious components reconstructed from non-smooth RCS data. Finally, the number of measurements M is determined automatically by the MATLAB-based RCS convergence script.

4.1 CS-Current Approach

First, we simulated a generic 4m x 4m plate at 300MHz with incident angles from $\theta = 0°$ to 360° and $\phi = 90°$. The geometry was created and meshed in newFASANT software, as shown in Figure 8. There are a total of n = 1600 rectangular surfaces (or meshes). Note that, depending on the basis expansion equations incorporated and the mesh density setting in different software, the number of meshes may vary, even for the same object at the same frequency. For example, newFASANT uses quadrilateral (four edges or sides) type of meshing method, while FEKO uses triangular-shaped meshing method as shown in Figure 9.

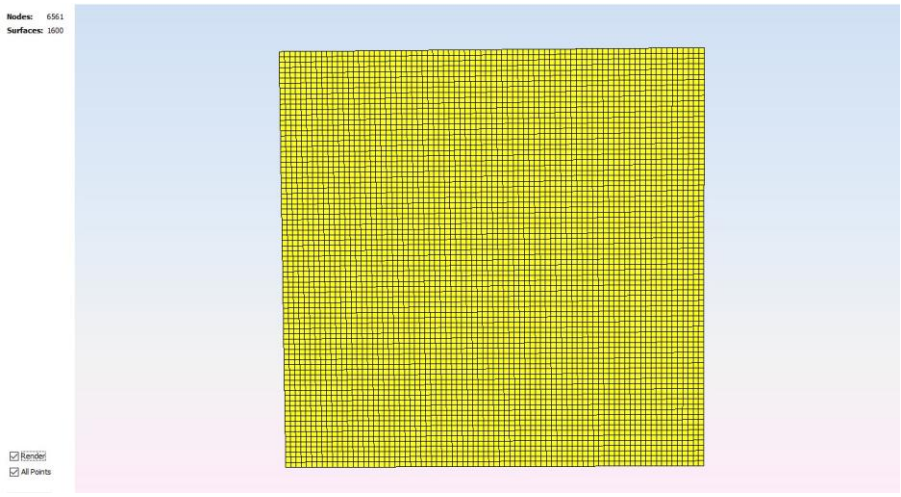

Figure 8 - 4m x 4m plate meshed in newFASANT

Also, newFASANT and FEKO use different basis expansion functions. For instance, instead of the rooftop basis expansion function used in newFASANT, FEKO uses Rao-Wilton Glisson (RWG) basis expansion function [42]. Note that, different meshing and basis expansion features do have an impact on the currents reconstruction quality since the sparsity (or compressibility) differs from signal to signal. Both software above provide built-in functionality to export and import currents in binary format. In this report, we focus on projects simulated using newFASANT software.

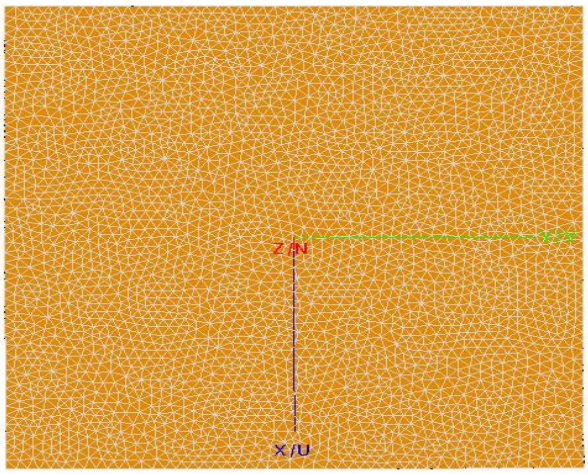

Figure 9 - 4m x 4m plate meshed in FEKO

Note that it is important to export the basis expansion current coefficients, which are the $I_k(\theta_i)$ used in the matrix equation, as some EM software also provide surface currents that can be confused with $I_k(\theta_i)$. The total number of surface currents is equal to the total number of meshes. However, due to the basis expansion function embedded in newFASANT, the total number of expansion coefficients is roughly twice the total number of meshes in newFASANT simulations. In the case of 4m x 4m plate simulated at 300MHz, there are k = 3120 basis expansion coefficients, which indeed almost doubles the number of meshes.

Table 5 - Performance of Reconstruction Algorithms at 1 and 0.5 Degrees of Angular Resolution

Reconstruction Algorithm	**1° Angular Resolution**		**0.5° Angular Resolution**	
	Error	Speed (s)	Error	Speed (s)
OMP	0.2094	72.0937	0.1420	181.9467
SpaRSA τ=0.0005	0.2081	525.9465	0.1357	720.3384
ROMP	0.3713	22.6415	0.3053	130.8816
CoSaMP	0.2632	118.5701	0.2046	190.3453

To examine the sparsity of $I_k(\theta_i)$, one can plot the currents concerning the range of incident angles. As shown in Figure 9, the currents at the 3120th patch seem to be noisy in the sense that many

spikes and discontinuities can be observed from a non-smooth signal. In comparison, the currents at the 9th patch exhibit in a smoother and more periodic manner compared to the currents the 3120th patch. However, the FFT domain current coefficients of the 3120th patch have few dominant coefficients and seem to be very compressible. The FFT of the currents of the 3120th patch is not as compressible as those in the 9th patch.

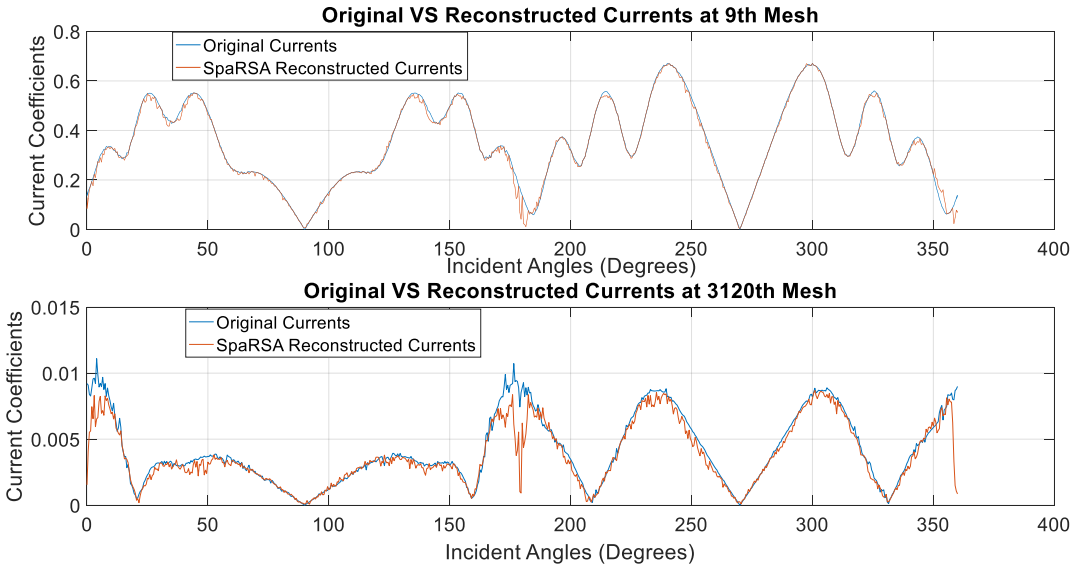

Figure 10 - Original VS Reconstructed Currents at the 9th (top) and 3120th mesh (bottom) of the plate with 0.5°resolution

In fact, we have several patches that contain less-than-sparse currents as those from the 3120th patch, especially near the edge of the plate. However, those currents are highly compressible, thus recoverable with a certain error rate. Currents like those from the edge patches have very low amplitudes, and thus inflict small impact on the overall RCS. Also, for RCS at each angle, there are 3120 of such currents. The contribution for a special case to the overall RCS is negligible.

As can be seen in Table 5, reconstruction accuracy improves as the angular resolution increases. Although OMP and SpaRSA both provide decent reconstruction accuracy, SpaRSA suffers more from the numerous iterations required for the CS-Current approach. However, for the following CS-RCS approach, only one iteration is required for signal reconstruction. Hence, the algorithm speed plays a significant role in CS-Current approach but is negligible in the CS-RCS approach.

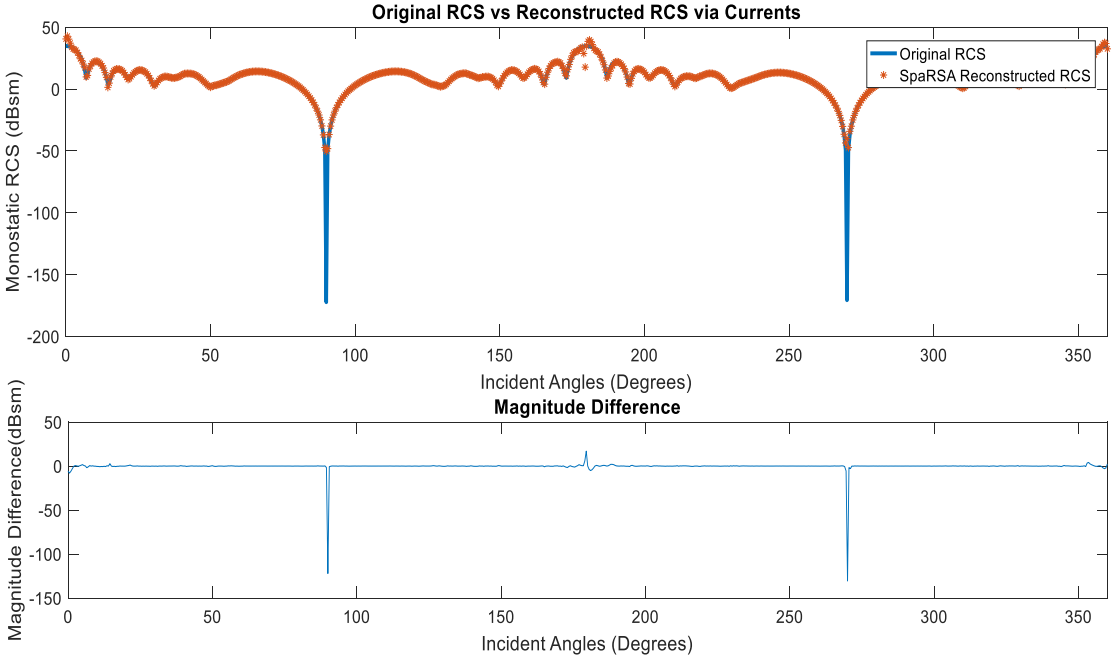

Figure 11 - Original vs SpaRSA Reconstructed RCS via Currents and Their Difference of the plate with 0.5°resolution

Figure 11 depicts that minor discrepancy can be found between the reconstructed and the original RCS at the two nulls around 90 and 260 degrees.

4.2 CS-RCS Approach

4.2.1 Missile

The geometry of a generic 3D missile is presented in Figure 12. The missile is 2.2m in length, 0.4m in width and 0.4m in depth. The surface of the generic missile, without the sharp corners commonly found on the fins, is composed of mostly flat surfaces where diffraction effect can be minimized. The missile's RCS was simulated using both MoM and PO at 1GHz in newFASANT from $\phi = 0°$ to 360° in the $\theta = 90°$ cutting plane with AR = 1° and AR =0.5°. The surface of the missile was meshed into 3639 quadrilateral patches. Unlike the CS-Current approach that reconstructs currents across all directions with respect to each patch, the RCS signal is reconstructed once for the entire surface of the objects.

The first step was to select an appropriate transformation basis, in which the RCS signal appears to be the most sparse or compressible. To focus solely on the impacts of different transformation

bases and reconstruction algorithms on the CS-RCS approach, a conservative number of measurements $M = N/2$ were used. As previously discussed, RCS signals are mostly found to have concise representation in the frequency domain. In this section, the compressibility of the RCS signals in DCT, DFT and Hermite Polynomial transformation bases are compared.

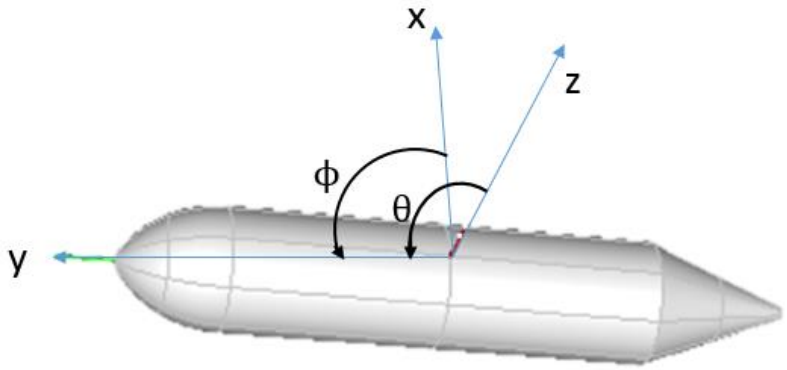

Figure 12 - 3D generic missile

4.2.1.1 1° Angular Resolution

As can be seen from Table 6, DFT generally provides the most accurate results, and Hermite Polynomial yields the largest reconstruction error. Among all reconstruction algorithms, the performance of SpaRSA remains superb and consistent throughout different transformation bases and frequencies.

Table 6 - Missile RCS Reconstruction Accuracy Comparisons between Different Bases and Algorithms at 1GHz with Angular Resolution = 1°

Hermite Polynomial/ Reconstruction algorithm	**Hermite Polynomial**	**DCT**	**DFT**
OMP	0.8668	0.2874	0.0803
ROMP	0.5544	0.7242	0.0849
CoSaMP	0.5615	0.3362	0.1396
BP	0.8343	0.2431	0.8615
SpaRSA	0.5490	0.2412	0.0797

Figure 13 depicts, graphically, the original monostatic RCS versus the reconstructed RCS using SpaRSA algorithm and DFT transformation matrix. The reconstructed RCS is mainly aligned with

the original RCS. Although the reconstructed signal misses the null at the incident angle around 220 degrees, it captures the decrease and the other nulls following the miss.

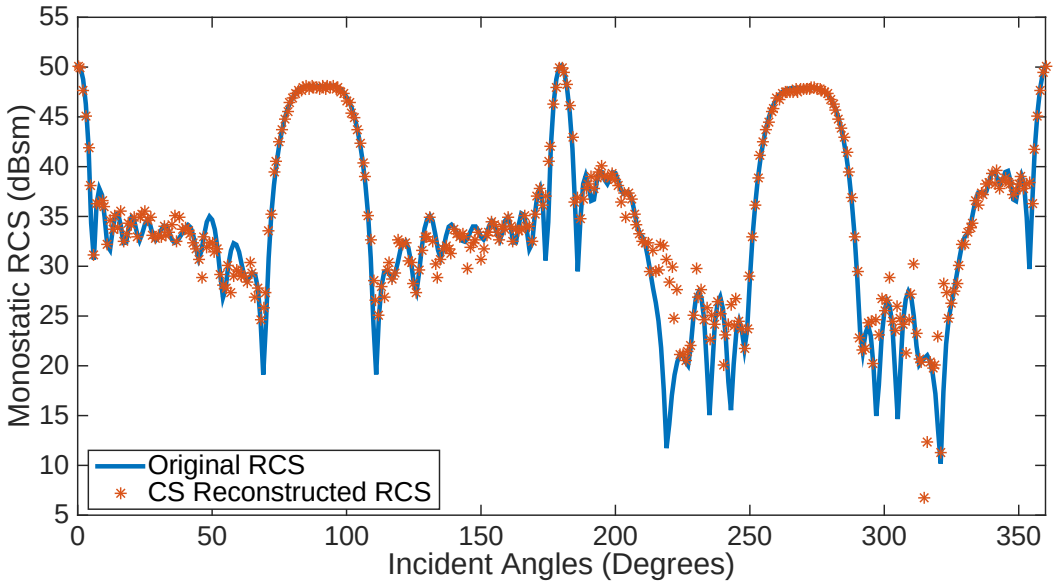

Figure 13 - RCS of generic missile versus recovered RCS via SpaRSA with 1-degree angular resolution at 1GHz; M=N/2=181 measurements were used for reconstruction

For generic objects with low structural complexity, such as the missile used in this section, even low angular resolution is capable of accurate signal recovery.

4.2.1.2 0.5° Angular Resolution

As can be seen in Figure 14, the SpaRSA reconstructed the RCS signal using 361 measurements largely resembles the original signal, with almost every peak and nulls aligned.

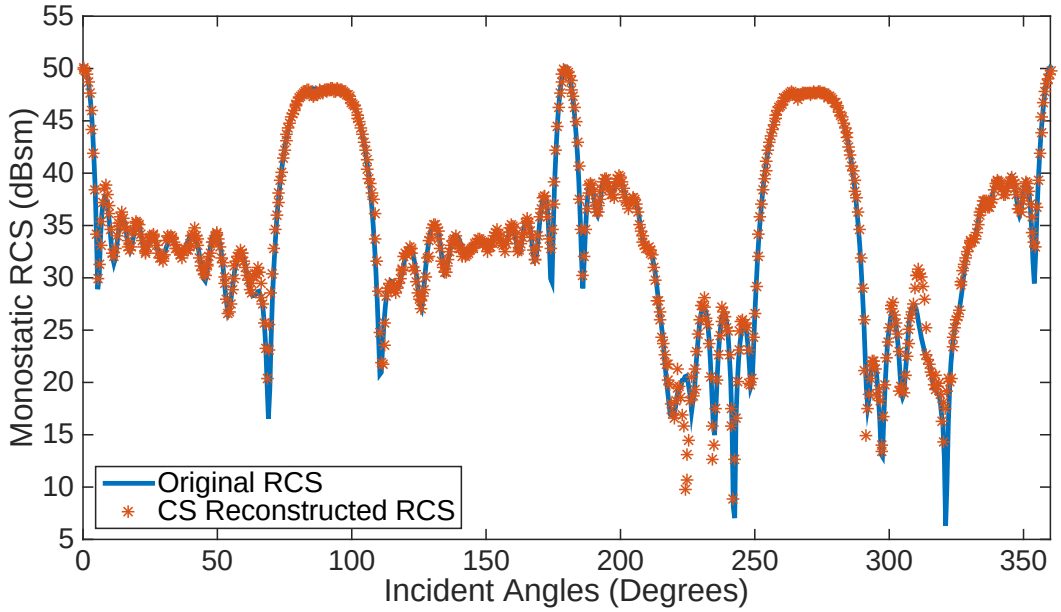

Figure 14 - RCS of generic missile versus recovered RCS via SpaRSA with 0.5-degree angular resolution at 1GHz; M=N/2=361 measurements were used for reconstruction

Figure 15 illustrates the exponential decay of the missile's RCS components in different transformation bases. As discussed in Chapter 2, higher compressibility results in a higher probability of better reconstruction accuracy. Clearly, the missile's RCS signal has the most concise representation under the DFT basis; the least compressible representation can be found in the Hermite basis.

Table 7 - Missile RCS Reconstruction Accuracy Comparisons between Different Bases and Algorithms at 1GHz with Angular Resolution = 0.5°

Hermite Polynomial/ Reconstruction algorithm	**Hermite Polynomial**	**DCT**	**DFT**
OMP	0.7276	0.1897	0.0503
ROMP	0.6709	0.2328	0.0377
CoSaMP	0.8559	0.1941	0.0834
BP	0.5827	0.2035	0.8939
SpaRSA	0.5461	0.2012	0.0413

From Table 10, one can conclude that the reconstruction accuracy improves as the angular resolution increases regardless of the transformation bases used to represent the signal. In fact, the DFT transformation basis offers the best reconstruction accuracy while Hermite suffers from properly recovering the signal.

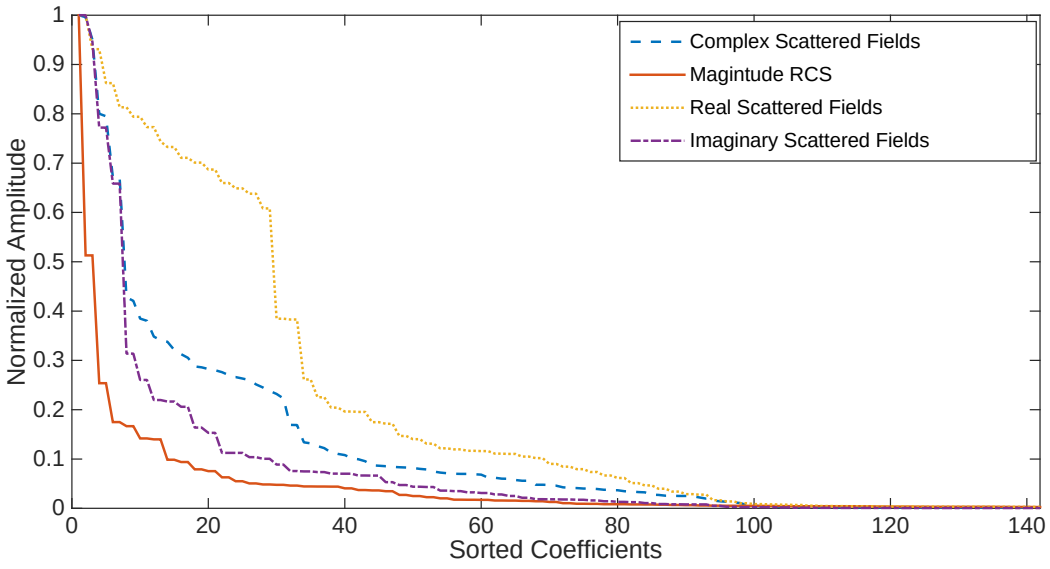

Figure 15 - The comparison of the compressibility of the missile's complex scattered fields vs. the real part of scattered fields, the imaginary part of scattered fields and the magnitude (RCS) at 1GHz with AR=0.5° (zoom in on the first 140 coefficients)

As Table 11 depicts, the reconstruction accuracy improves, as the regularization parameter τ described in equation (3-20) being fine-tuned. Theoretically, as the simulation data are free of noise corruption, it is reasonable for τ to be small. However, as τ decreases, it reaches diminishing return where the trade-off between the accuracy and run-time becomes more apparent. SpaRSA not only controls the noise level but also removes the spurious components, which are essentially the unwanted recovery artifacts that are normally generated during improper signal reconstruction. Like most reconstruction algorithms, SpaRSA iterates through an increasingly accurate signal estimation by distinguishing the leading signal components from spurious components [27].

The regularization parameter τ serves as a warm start that provides competitive reconstruction speed and accuracy with minimum *a priori* knowledge. The process of fine-tuning this τ is far less tedious than having to guess the sparsity of the signal for different objects, in different frequencies and with different angular resolutions.

Table 8 - Accuracy Comparison of Different Transformation Bases using Various Regularization Parameters

Regularization τ	DCT error	DFT error
0.05	0.31320	0.25291
0.005	0.21365	0.06224
0.0005	0.21403	0.04103
0.00005	0.24342	0.03293

As can be seen in Table 9, the reconstruction error of the RCS signal is significantly lower than the complex scattered fields or their real and imaginary parts separately. To understand this phenomenon, the compressibility of the signals of interest is examined by 1) normalizing the amplitude of each signal 2) sorting their coefficients represented in the same transformation basis from the largest to the smallest. As a result, Figure 15 depicts, graphically, the compressibility of the RCS signal of the generic missile with 0.5 degrees of angular resolution and simulated at 400MHz. The most rapid decay of coefficients can be observed in the RCS signal.

Table 9 - Reconstruction Accuracy of RCS vs Complex Scattered Fields at 1GHz with Angular Resolution = 0.5°

Signal of Interest	SpaRSA τ=0.0005	OMP
RCS	0.0413	0.0828
Complex Scattered Fields	0.2898	0.2952
Real Scattered Fields	0.3441	0.3576
Imaginary Scattered Fields	0.2980	0.3015

As mentioned in Chapter 3, a MATLAB function was developed to automatically accumulate the number of measurements until the reconstructed RCS converges. To initiate the program, a fixed number of measurements, as well as the reconstructed RCS, was first generated. Then, according to the knowledge and experience of the operator, a second RCS was generated using the second set of measurements that are not redundant with the initial one. The convergence of the RCS was monitored by taking the Frobenius norm of the two reconstructed RCSs. As the iteration continues, the error decreases and the RCS eventually converge. In the case of the simulation of the missile's

RCS at 1GHz with 0.5° angular resolution, its RCS converges with only 252 measurements. As a result, the Frobenius error of the RCS is 0.0483, which is very close to 0.0413 when 361 measurements were used. Therefore, 35% of the original signal length (N=721) was required for near-optimal RCS approximation of the missile under the situation described. Based on the observations of the reconstructed RCS, one can conclude that the generic missile provides smooth signals even at 1GHz frequency.

Table 10 - Missile and plate CPU speed performance

Object	**Approach & algorithm**	**Angular Resolution (°)**	**Frequency (MHz)**	**NewFASANT Run-time (s)**	**CS Run-time(s)**
Plate	CS-Current & OMP	1	300	715	422
		0.5	300	1078	711
Missile	CS-RCS & SpaRSA	1	400	153	58
		0.5	400	548	261

By comparing the newFASANT and the CS run-times listed in Table 10, one can tell the superior efficiency of the CS-RCS approach compared to the CS-Current approach. Despite that, the plate being the less structurally complex one of the two objects, the run-time that was taken to compute the RCS of the plate using the CS-Current approach is significantly more than that of the missile using the CS-RCS approach.

4.3 King Air Aircraft

This section provides simulation results of CS-based RCS computation of a Canadian King Air aircraft, which was 3D laser-scanned and imported into AutoCAD by DRDC Ottawa. Therefore, the original 3D CAD model highly resembles the surface detail of the actual King Air aircraft. In order to be able to perfectly render the 3D CAD model in newFASANT or other commercial electromagnetic solvers, some disconnecting surfaces in the original 3D model were partially discarded and smoothed out. As a result, the KingAir model (15.3 x 10.8 x 4.7 m^3) retains fine details of the aircraft, including the propellers and intakes and its RCS was computed at 1 and

2GHz for N = 721,1441 and 2881 incident angles or at the angular resolution equal to 0.5, 0.25 and 0.125 degrees, respectively.

The under-sampled RCSs were acquired from M random measurements over $\phi = 0°$ to $360°$ in the $\theta = 90°$ cutting plane. The numbers of measurements were determined using the RCS Convergence MATLAB script. Since EM scattering problems only feature signals of finite length, the discrete Fourier transform (DFT) is the natural choice for EM related CS applications. However, DFT works well primarily with smooth or modulated signals[39]. For a complex conducting body such as the KingAir aircraft, 1-degree angle resolution is incapable of representing its true RCS at microwave frequencies.

As object complexity and frequency increase, the RCS of a complex object becomes coarser and less smooth. Consequently, even with increased measurements, the under-sampled RCS (1) cannot represent the object's true radar signature, and (2) deteriorates the signal compressibility in the Fourier basis[39]. Thus, a finer spatial (or angular) resolution is needed to properly resemble the smooth and continuous characteristics of the KingAir RCS. The process of the proposed CS-based method is twofold: the commercial EM software newFASANT computes the far-field RCS sampled at M <<N incident angles using the Physical Optics solver. Then a developed MATLAB code recovers the full-length RCS using the reconstruction algorithm.

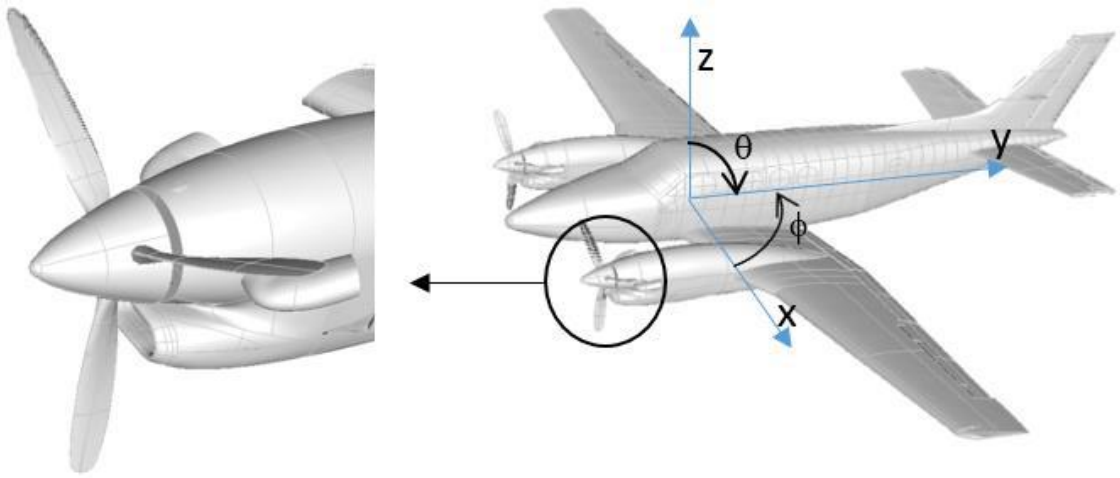

Figure 16 - King Air 3D Model

The RCS was reconstructed by solving a convex optimization problem addressed in equation (3-18) known as Basis Pursuit De-noising using the sparse reconstruction by separable approximation (SpaRSA). One can calculate the reconstruction error using the Frobenius norm of the vector signal:

$$err = \frac{\|\boldsymbol{RCS}^{CS} - \boldsymbol{RCS}^{PO}\|_F}{\|\boldsymbol{RCS}^{PO}\|_F} \qquad (4-1)$$

where $\boldsymbol{RCS}^{CS}$ is the reconstructed signal by SpaRSA and $\boldsymbol{RCS}^{PO}$ is the original RCS of the King Air aircraft. Through numerous experiments, we found that the RCS signals are generally compressible in DFT and DCT domains. However, the DFT domain offers sparser and slightly better reconstruction quality. As explained in Chapter 3, the iterative soft thresh-holding based SpaRSA algorithm offers fewer reconstruction errors than the other three reconstruction algorithms. RCS data is spatially dependent with a combination of regional events where different regions resemble a different group structure. Certain group structure may be better reconstructed using l_1 regularizer where others are better off with l_2 regularizer as described in [27]. Therefore, SpaRSA reduces recovery artifacts and lead to a more robust recovery.

Table 11 - Reconstruction Errors of Different Algorithms for Different Angular Resolution (AR) using CS-RCS approach combined with the PO solver in newFASANT

Frequency and Angular Resolution	Reconstruction Methods			
	SpaRSA	***OMP***	***ROMP***	***CoSaMP***
1GHz AR=0.5°	0.2913	0.3413	0.3519	0.3518
1GHz AR=0.25°	0.2337	0.2884	0.2954	0.3026
1GHz AR=0.125°	0.1672	0.2691	0.2914	0.2638
2GHz AR=0.5°	0.3236	0.3696	0.3645	0.3641
2GHz AR=0.25°	0.3823	0.4178	0.4145	0.4258
2GHz AR=0.125°	0.2541	0.3289	0.3341	0.3507
5GHz AR=0.1°	0.3059	0.3562	0.3506	0.3733

As can be seen in Table 11, SpaRSA stands out, once again, as the ideal reconstruction algorithm, which offers more robustness in preventing sampling artifacts and does not require a priori knowledge of the signal sparsity or compressibility.

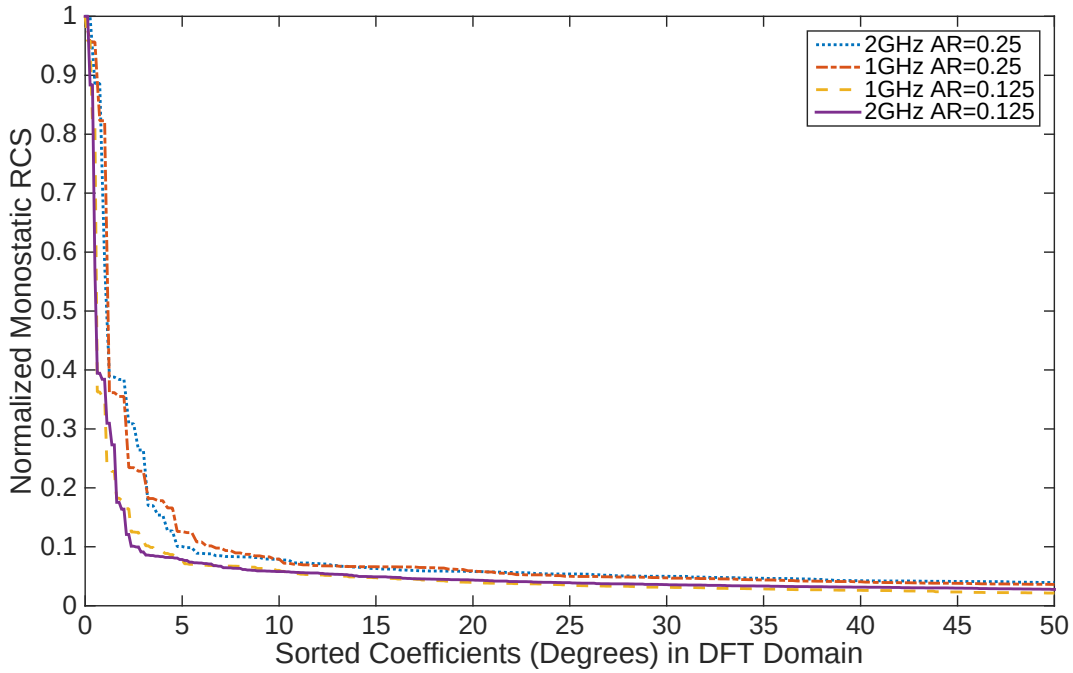

Figure 17 - *Sorted RCS coefficients in the DFT domain using a different number of incident angles, N. The picture is zoomed in on the 50 largest coefficients*

Figure 17 shows that as the angular resolution increases, the RCS coefficients in DFT basis decay faster, contributing to greater compressibility and better reconstruction accuracy. However, with the same angular resolution, as the frequency increases, the compressibility decrease.

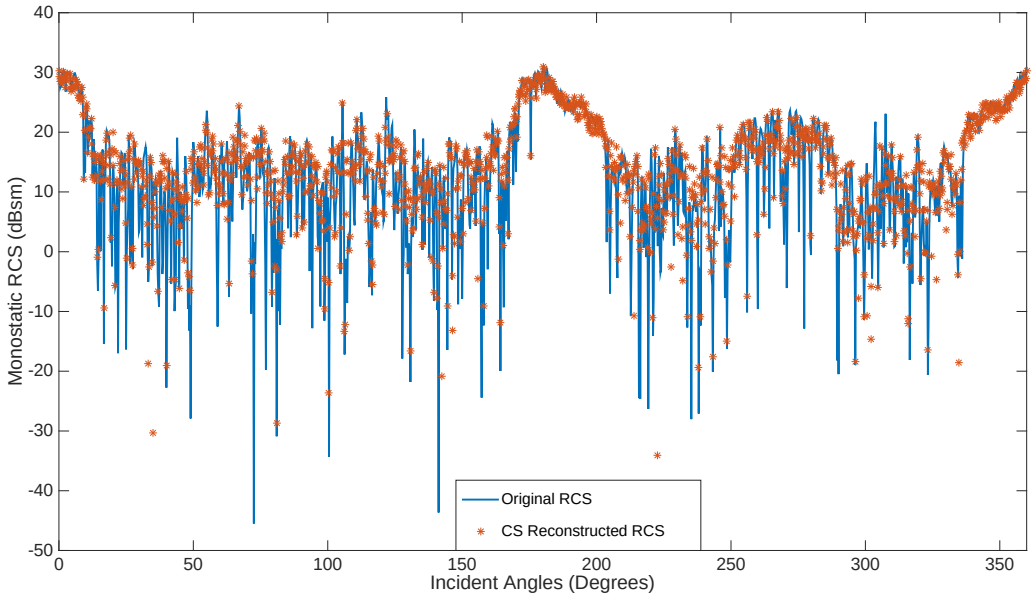

Figure 18 - Original RCS of King Air versus the RCS recovered via SpaRSA at 0.25 degrees angular resolution with M=693 measurements at 1GHz

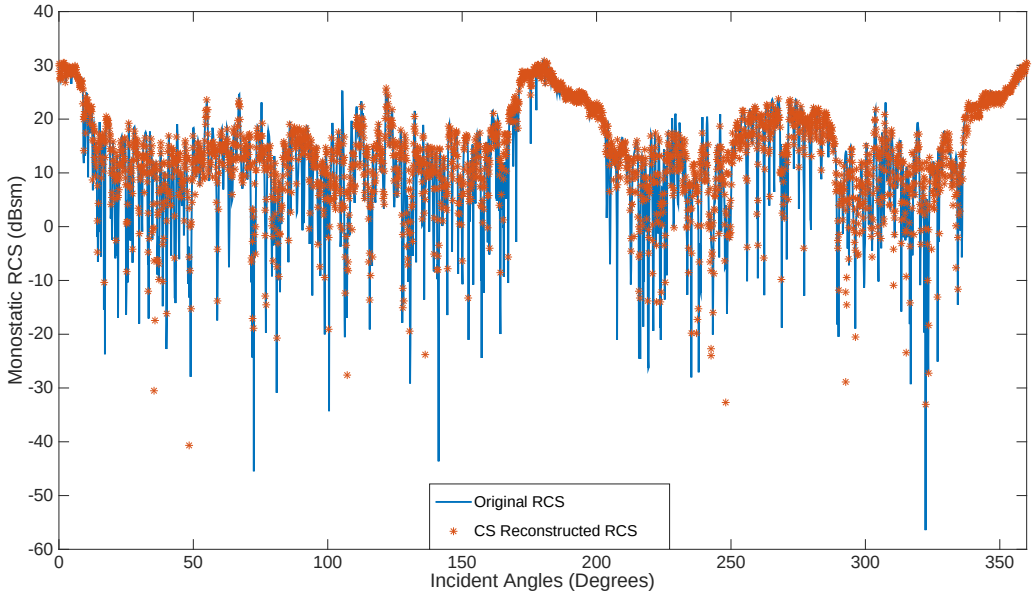

Figure 19 - Original RCS of King Air versus the RCS recovered via SpaRSA at 0.125 degrees angular resolution with M=1296 measurements at 1GHz

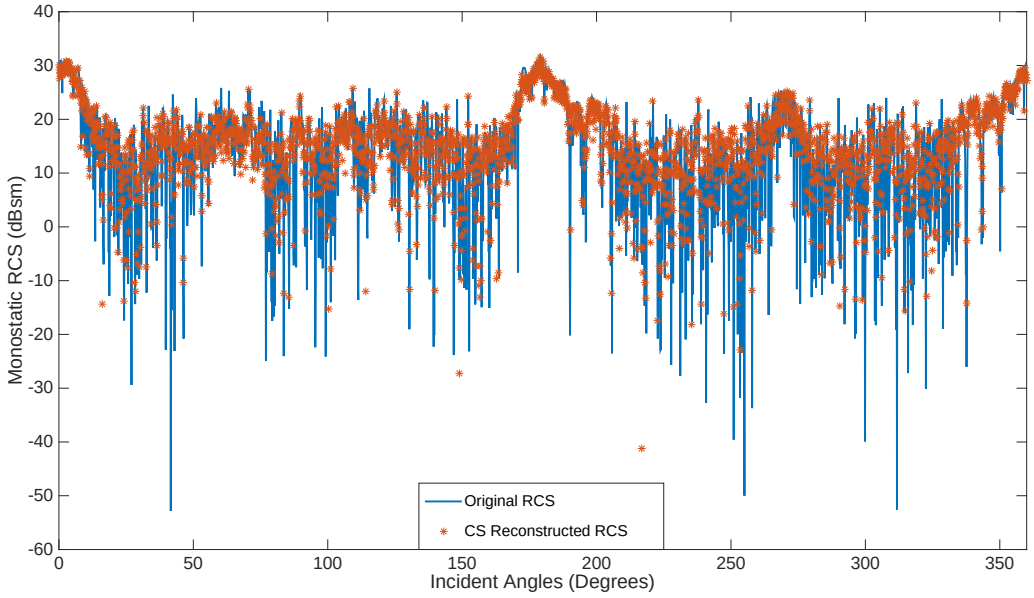

Figure 20- Original RCS of King Air versus the RCS recovered via SpaRSA at 0.125 degrees angular resolution with M =1411 measurements at 2GHz

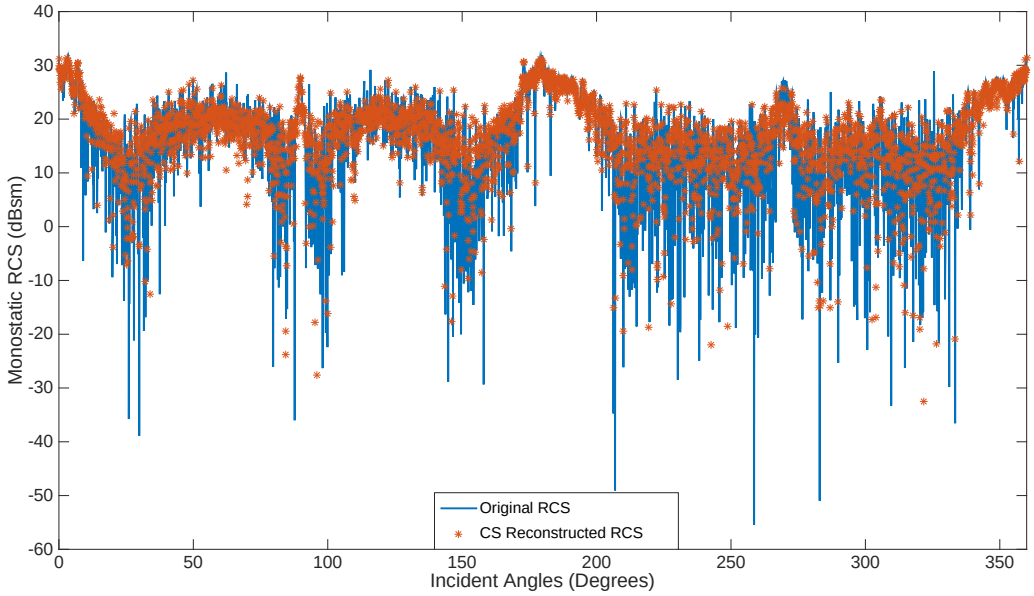

Figure 21 - Original RCS of King Air versus the RCS recovered via SpaRSA at 0.1 degrees angular resolution with M = 1800 measurements at 5GHz

As shown in Figures 18, 19, 20 and 21, the recovered RCS signals using AR = 0.125° at 1 and 2 GHz, and AR = 0.1° at 5GHz are in good agreements with the nulls and peaks of the original RCSs. As proved by the numerical results presented, the compressibility of RCS signals decreases as the simulation frequency and structurally complexity increase. To compensate for the

deterioration of compressibility, this thesis recommends SpaRSA reconstruction algorithm with improved angular resolution. From empirical results, SpaRSA has shown its impressive capability of handling reconstruction artifacts and recovering compressible signals. By comparing Tables 5,6 and 11, one can see that the gap in reconstruction accuracy between SpaRSA and the greedy algorithms expands drastically, as the structure-complexity and frequency increase.

Naturally, as a result of increased simulation frequency, the size of a given object's surface becomes relatively larger compared to the wavelength of the incident waves. For example, for the 4m by 4m plate simulated at 300MHz, the RCS at a normal direction is $201m^2$, which is more than a dozen times bigger than the physical area of the plate. In fact, [29] suggests a small step in the aspect direction may cause a fluctuation of tens of decibels in RCS. This phenomenon can be observed by comparing Figure 18, 19, 20 and 21, where each RCS plot is slightly different since the angular resolution and simulation frequency are different. Therefore, to properly capture the RCS of a complex target, especially at high frequencies, the RCS should be simulated with fine precision captured by a proper angular resolution. Notwithstanding this phenomenon, finer angular resolution significantly improves the compressibility of RCS signals. In consequence of improved compressibility, the RCS signal's reconstruction accuracy increases.

Table 12 - NewFASANT Run-Time VS CS-RCS Run-Time

Frequency	Original signal length	CS signal length	Original run-time (mins)	CS-RCS run-time (mins)
1GHz	N=1441 AR=0.25°	N=693	322.5	159.0
1GHz	N=2881 AR=0.125°	N=1296	790.9	386.4
2GHz	N=1441 AR=0.25°	N=719	1320.1	646.8
2GHz	N=2881 AR=0.125°	N=1411	2112.3	1190.6

As can be seen from Table 12, the RCS data of the King Air aircraft was simulated using newFASANT and its PO EM solver on a Supermicro Server with the following spec:

- CPU: Intel Xeon CPU E3-1535M 2.90GHz
- Number of Cores: 8
- Installed Memory (RAM): 32GHz

The CS-RCS saves 50.6%, 51.1%, 51.0 and 43.6% run-time for simulations using AR = 0.25° and 0.125° at 1GHz and AR = 0.25° and 0.125° at 2GHz, respectively.

4.4 Conclusion

This chapter demonstrated the numerical results of reconstructed and original RCS of plate, missile and Kiang Air aircraft at various frequencies and angular resolutions using the CS-Current and CS-RCS approach combined with newFASANT. Results show that, as structural-complexity of the geometry and simulation frequency increase, the RCS signal becomes less compressible, which deteriorate the reconstruction accuracy. With increased angular resolution, SpaRSA algorithm was able to eliminate reconstruction artifacts and improve the accuracy of reconstructed RCS of the structurally complex object at high frequencies. Finally, CS-RCS was proven to improve the RCS computation time significantly.

Chapter 5 Conclusions and Future Work

5.1 Conclusions

This thesis discussed the fundamentals of compressive sensing and its applications in computational electromagnetics. It also analyzed various approaches that exploit CS to improve the computation efficiency of RCS of generic objects. A new CS-RCS approach combined with MATLAB-based SpaRSA algorithm was proposed to improve the efficiency of the EM commercial software newFASANT in solving EM scattering problems of both generic and complex real-life objects at microwave frequencies (300MHz to L-band) using PO solver. Instead of having to extract the currents or scattered field data just to compute the RCS of an object, the CS-RCS directly utilizes RCS signals that promote better compressibility and recovery accuracy than the conventional CS approaches.

The CEM signals of interest, including the current, electric-field and RCS signals were compared against various transformation bases, including DFT, DCT and Hermite transformation bases. Results demonstrated that the RCS/DFT pair exhibits the highest compressibility. Besides the well-known transformation matrix, this work associates, for the first time, the RCS resolution, frequency and structural-complexity as the determining factors of a given RCS signal's compressibility, which contributes significantly to the possibility and accuracy of signal reconstruction.

The SpaRSA algorithm, which is an accelerated iterative thresholding algorithm, demonstrated superior stability that drastically improves the reconstruction accuracy of RCS signals without sacrificing the runtime, when compared to popular Greedy reconstruction algorithms, such as OMP, CoSaMP and ROMP. The proposed CS-RCS method (when incorporated with SpaRSA algorithm and the measurement matrix composed of uniform sampling matrix and DFT transformation matrix) is capable of improving the efficiency of RCS computation of complex targets in microwave frequencies with satisfactory accuracy. Also, The CS-RCS saves 50.6%, 51.1%, 51.0 and 43.6% run-time for simulations using AR = 0.25° and 0.125° at 1GHz and AR = 0.25° and 0.125° at 2GHz, respectively.

5.2 Future work

Despite being the most frequency-sparse transformation basis out of the three bases presented in the thesis, DFT only provides the sparsest representation for sinusoids with an integer frequency. If the frequency is not an integer, the signal does not entirely align with the centre of the DFT's frequency grid and cannot be properly interoperated. This issue has been addressed as "spectral leakage problem" in [22]. In order for all DFT coefficients to be sparse, the sinusoid frequencies specified in equation (2-11) must be integral of the form of $\frac{2\pi n}{N}$, with n an integer. Also, [22] proposed a spectral compressive sensing method which adopts a model-based framework along with a spectral iterative hard thresholding reconstruction algorithm to tackle the leakage problem. In [43], this phenomenon is mentioned as the mismatch between the assumed $\boldsymbol{\Psi_0}$ and the actual bases for sparsity $\boldsymbol{\Psi_1}$. The hypothesized $\boldsymbol{\Psi_0}$, for example, can be the ideal form of DFT, and $\boldsymbol{\Psi_1}$ is the realistic physical field determined by frequencies that do not necessarily align with the gridding point of DFT [43]. Consequently, the mismatched basis can be represented as $\boldsymbol{\Psi} = \boldsymbol{\Psi_0^{-1}\Psi_1}$. This can be further explored.

However, as discussed in Chapter 2, the incoherent property between the sensing matrix and the transformation matrix is theoretically powerful. So, research has shown that structured measurement systems offer better efficiency and accuracy for certain types of signals than the traditional unstructured measurement systems. The structured measurement systems provide robust recovery of K-structured sparse signal using tailored thresholding and greedy reconstruction algorithms for further works, scattering signals across more variety of objects will be studied.

In [44], the authors proposed a new sampling scheme where a given signal is sampled non-linearly using a structured signal model in a union of subspaces. This method works well with certain types of signals whose non-zero components concentrate in fixed blocks. An $l_2/\ l_1$ mixed minimization algorithm was developed to determine the block-sparse vector corresponding to a given set of measurements. [45] studied two structured models: tree structure that can be commonly identified from wavelet coefficients of imaging signals and the aforementioned block sparse model. In addition, CoSaMP and Iterative Hard-Thresholding algorithms are specially tailored to deal with the two structured models. RCS signals can often found to be sparse with non-zero coefficients

concentrate both in the lower and upper end of the spectrum in Fourier Transform domain. That being said, the block-structure incorporated algorithms may facilitate the reconstruction process, if the signal sparsity can be accurately predicted from future research.

However, most methods with regards to tackle a spectral leakage problem require additional *a priori* knowledge, such as the sparsity, structure and, even, the estimated frequencies of sinusoids of the signal. For RCS signals in CEM applications, the model or structure of the signals vary drastically with respect to different objects and frequencies – let alone the sparsity is unpredictable.

References

[1] M. F. Duarte *et al.*, "Single-pixel imaging via compressive sampling," *IEEE Signal Process. Mag.*, vol. 25, no. 2, pp. 83–91, Mar. 2008.

[2] D. L. Donoho, "Compressed sensing," *IEEE Trans. Inf. Theory*, vol. 52, no. 4, pp. 1289–1306, Apr. 2006.

[3] E. J. Candes and T. Tao, "Near-Optimal Signal Recovery From Random Projections: Universal Encoding Strategies?," *IEEE Trans. Inf. Theory*, vol. 52, no. 12, pp. 5406–5425, Dec. 2006.

[4] E. J. Candès, J. K. Romberg, and T. Tao, "Stable signal recovery from incomplete and inaccurate measurements," *Commun. Pure Appl. Math.*, vol. 59, no. 8, pp. 1207–1223, Aug. 2006.

[5] E. J. Candes, J. Romberg, and T. Tao, "Robust uncertainty principles: exact signal reconstruction from highly incomplete frequency information," *IEEE Trans. Inf. Theory*, vol. 52, no. 2, pp. 489–509, Feb. 2006.

[6] R. Baraniuk, "Compressive Sensing [Lecture Notes]," *IEEE Signal Process. Mag.*, vol. 24, no. 4, pp. 118–121, Jul. 2007.

[7] M. Lustig, D. Donoho, and J. M. Pauly, "Sparse MRI: The application of compressed sensing for rapid MR imaging," *Magn. Reson. Med.*, vol. 58, no. 6, pp. 1182–1195, Dec. 2007.

[8] F. Herrmann, M. Friedlander, and O. Yilmaz, "Fighting the Curse of Dimensionality: Compressive Sensing in Exploration Seismology," *IEEE Signal Process. Mag.*, vol. 29, no. 3, pp. 88–100, May 2012.

[9] S.-R. Chai and L.-X. Guo, "Compressive Sensing for Monostatic Scattering From 3-D NURBS Geometries," *IEEE Trans. Antennas Propag.*, vol. 64, no. 8, pp. 3545–3553, Aug. 2016.

[10] L. Carin, D. Liu, and Y. Xue, "In Situ Compressive Sensing," in *2007 2nd IEEE International Workshop on Computational Advances in Multi-Sensor Adaptive Processing*, 2007, pp. 105–108.

[11] C. A. Balanis, *Advanced engineering electromagnetics*. John Wiley & Sons, 2012.

[12] R. F. Harrington and IEEE Antennas and Propagation Society., *Field computation by moment methods*. IEEE Press, 1993.

[13] E. Garcia, C. Delgado, I. G. Diego, and M. F. Catedra, "An Iterative Solution for Electrically Large Problems Combining the Characteristic Basis Function Method and the Multilevel Fast Multipole Algorithm," *IEEE Trans. Antennas Propag.*, vol. 56, no. 8, pp. 2363–2371, Aug. 2008.

[14] M.-J. Algar, L. Lozano, J. Moreno, I. González, and F. Cátedra, "An efficient hybrid technique in RCS predictions of complex targets at high frequencies," *J. Comput. Phys.*, vol. 345, pp. 345–357, Sep. 2017.

[15] S.-R. Chai, L.-X. Guo, K. Li, and L. Li, "Combining CS With FEKO for Fast Target Characteristic Acquisition," *IEEE Trans. Antennas Propag.*, vol. 66, no. 5, pp. 2494–2504, May 2018.

[16] S.-R. Chai and L.-X. Guo, "Integration of CS into MoM for Efficiently Solving of Bistatic Scattering Problems," *IEEE Antennas Wirel. Propag. Lett.*, vol. 15, pp. 1771–1774, 2016.

[17] J. A. Tropp and A. C. Gilbert, "Signal Recovery From Random Measurements Via Orthogonal Matching Pursuit," *IEEE Trans. Inf. Theory*, vol. 53, no. 12, pp. 4655–4666, Dec. 2007.

[18] A. Massa, P. Rocca, and G. Oliveri, "Compressive sensing in electromagnetics - A review," *IEEE Antennas and Propagation Magazine*, vol. 57, no. 1. IEEE Computer Society, pp. 224–238, 01-Feb-2015.

[19] E. J. Candès, J. Romberg, and T. Tao, "Robust uncertainty principles: Exact signal reconstruction from highly incomplete frequency information," *IEEE Trans. Inf. Theory*, 2006.

[20] Y. Tsaig and D. L. Donoho, "Extensions of Compressed Sensing," 2004.

[21] E. J. Candes and T. Tao, "Decoding by Linear Programming," *IEEE Trans. Inf. Theory*, vol. 51, no. 12, pp. 4203–4215, Dec. 2005.

[22] M. F. Duarte and R. G. Baraniuk, "Spectral compressive sensing," *Appl. Comput. Harmon. Anal.*, vol. 35, no. 1, pp. 111–129, Jul. 2013.

[23] E. J. Candès, "The restricted isometry property and its implications for compressed sensing," *Comptes Rendus Math.*, vol. 346, no. 9–10, pp. 589–592, May 2008.

[24] E. J. Candes and M. B. Wakin, "An Introduction To Compressive Sampling," *IEEE Signal Process. Mag.*, vol. 25, no. 2, pp. 21–30, Mar. 2008.

[25] D. L. Donoho and X. Huo, "Uncertainty principles and ideal atomic decomposition," *IEEE Trans. Inf. Theory*, vol. 47, no. 7, pp. 2845–2862, 2001.

[26] S. Qaisar, R. M. Bilal, W. Iqbal, M. Naureen, and S. Lee, "Compressive sensing: From theory to applications, a survey," *J. Commun. Networks*, vol. 15, no. 5, pp. 443–456, Oct. 2013.

[27] S. J. Wright, R. D. Nowak, and M. A. T. Figueiredo, "Sparse Reconstruction by Separable Approximation," *IEEE Trans. SIGNAL Process.*, vol. 57, no. 7, p. 2479, 2009.

[28] S. Stanković, L. Stanković, and I. Orović, "Compressive Sensing Approach in the Hermite Transform Domain," *Math. Probl. Eng.*, vol. 2015, pp. 1–9, Dec. 2015.

[29] W.-K. Chen, *The electrical engineering handbook*. Elsevier Academic Press, 2005.

[30] Ming Sheng Chen, Fa Lin Liu, Hong Mei Du, and Xian Liang Wu, "Compressive Sensing for Fast Analysis of Wide-Angle Monostatic Scattering Problems," *IEEE Antennas Wirel. Propag. Lett.*, vol. 10, pp. 1243–1246, 2011.

[31] R. J. Burkholder, A. N. O'Donnell, W. O. Coburn, and C. J. Reddy, "Sparse basis expansions for compressive sensing of electromagnetic scattering patterns computed using iterative physical optics," in *2012 International Conference on Electromagnetics in Advanced Applications*, 2012, pp. 434–437.

[32] M. F. Duarte and Y. C. Eldar, "Structured Compressed Sensing: From Theory to Applications," *IEEE Trans. Signal Process.*, vol. 59, no. 9, pp. 4053–4085, Sep. 2011.

[33] D. Needell and J. A. Tropp, "CoSaMP: Iterative signal recovery from incomplete and inaccurate samples," *Appl. Comput. Harmon. Anal.*, vol. 26, no. 3, pp. 301–321, May 2009.

[34] E. J. Candes and T. Tao, "Near-Optimal Signal Recovery From Random Projections: Universal Encoding Strategies?," *IEEE Trans. Inf. Theory*, vol. 52, no. 12, pp. 5406–5425, Dec. 2006.

[35] S. P. Boyd and L. Vandenberghe, *Convex optimization*. Cambridge University Press, 2004.

[36] M. Merritt and Y. Zhang, "Interior-Point Gradient Method for Large-Scale Totally Nonnegative Least Squares Problems," *J. Optim. Theory Appl.*, vol. 126, no. 1, pp. 191–202, Jul. 2005.

[37] A. Beck and M. Teboulle, "A Fast Iterative Shrinkage-Thresholding Algorithm for Linear Inverse Problems," *SIAM J. Imaging Sci.*, vol. 2, no. 1, pp. 183–202, Jan. 2009.

[38] Má. A. T. Figueiredo, R. D. Nowak, and S. J. Wright, "Gradient Projection for Sparse Reconstruction: Application to Compressed Sensing and Other Inverse Problems," *IEEE J. Sel. Top. Signal Process.*, vol. 1, no. 4, pp. 586–597, Dec. 2007.

[39] D. Xu, Y. Huang, and J. U. Kang, "Real-time compressive sensing spectral domain optical coherence tomography.," *Opt. Lett.*, vol. 39, no. 1, pp. 76–9, Jan. 2014.

[40] S. G. Mallat and Z. Zhang, "Matching Pursuits With Time-Frequency Dictionaries," *IEEE Trans. Signal Process.*, vol. 41, no. 12, pp. 3397–3415, 1993.

[41] D. Needell and R. Vershynin, "Uniform Uncertainty Principle and signal recovery via Regularized Orthogonal Matching Pursuit," Jul. 2007.

[42] S. Rao, D. Wilton, and A. Glisson, "Electromagnetic scattering by surfaces of arbitrary shape," *IEEE Trans. Antennas Propag.*, vol. 30, no. 3, pp. 409–418, May 1982.

[43] Y. Chi, L. L. Scharf, A. Pezeshki, and A. R. Calderbank, "Sensitivity to Basis Mismatch in Compressed Sensing," *IEEE Trans. Signal Process.*, vol. 59, no. 5, pp. 2182–2195, May 2011.

[44] Y. C. Eldar and M. Mishali, "Robust Recovery of Signals From a Structured Union of Subspaces," *IEEE Trans. Inf. Theory*, vol. 55, no. 11, pp. 5302–5316, Nov. 2009.

[45] R. G. Baraniuk, V. Cevher, M. F. Duarte, and C. Hegde, "Model-Based Compressive Sensing," *IEEE Trans. Inf. Theory*, vol. 56, no. 4, pp. 1982–2001, Apr. 2010.